The G3BP Stress-Granule Proteins Reinforce the Translation Program of the Integrated Stress Response

Jarrett Smith[1,2,3] & David P. Bartel[1,2,3]

[1]Howard Hughes Medical Institute and [2]Whitehead Institute for Biomedical Research, 9 Cambridge Center, Cambridge, MA 02142, USA

[3]Department of Biology, Massachusetts Institute of Technology, Cambridge, MA 02139, USA

Correspondence: dbartel@wi.mit.edu

ABSTRACT

When mammalian cells are exposed to extracellular stress, they coordinate the condensation of stress granules (SGs) through the action of key nucleating proteins G3BP1 and G3BP2 (G3BPs) and, simultaneously, undergo a massive reduction in translation.[1-5] Although SGs and G3BPs have been linked to this translation response, their overall impact has been unclear. Here, we investigate the longstanding question of how, and indeed whether, G3BPs and SGs shape the stress translation response. We find that SGs are enriched for mRNAs that are resistant to the stress-induced translation shutdown. Although the accurate recruitment of these stress-resistant mRNAs does require the context of stress, a combination of optogenetic tools and spike-normalized ribosome profiling demonstrates that G3BPs and SGs are necessary and sufficient to both help prioritize the translation of their enriched mRNAs and help suppress cytosolic translation. Together these results support a model in which G3BPs and SGs reinforce the stress translation program by prioritizing the translation of their resident mRNAs.

INTRODUCTION

When cells are exposed to environmental stresses, including oxidative stress, high temperature, harmful chemicals, and viral infection, the cells initiate the integrated stress response (ISR).[5-8] This response integrates signals from different stress sensors and ultimately results in reduced global translation, through phosphorylation of a critical translation initiation factor eif2α.[5-9] At the same time, select mRNAs continue to be translated or even undergo enhanced translation to help cope with and recover from the stress, whereas mRNAs whose products are energetically expensive for the cell are especially sensitive to down regulation.[6,8,10-13] During this dramatic alteration of the translation state, cytoplasmic puncta known as stress granules (SGs) form through the process of liquid-liquid phase separation.[2-5,10,14-16] These granules are non-membrane-bound collections of RNA-binding proteins, mRNAs, and translation machinery.[1,5,15,17-19] Although SGs contain a diverse proteome, they require the RNA-binding proteins G3BP1 and G3BP2 (G3BPs) for their formation.[1,2] Both SGs and G3BPs have been hypothesized to play roles in translation,[1,20-23] but their precise impacts on translation during the stress response are not well understood.

Because they are highly enriched for translation machinery and form concurrently with translation shutdown, SGs were originally hypothesized to be required for the dramatic translation shutdown observed during the ISR.[20,24,25] However, more recent studies indicate that SGs are not required for the massive reduction in translation that occurs during the ISR; G3BP KO cell lines, which are devoid of microscopically visible stress granules, still undergo the eif2α-dependent translation reduction associated with the ISR.[1,26]

Because the formation of SGs is enhanced by polysome collapse, and SGs are enriched in small ribosomal subunits but not large ribosomal subunits, SGs are also proposed to simply be sites of devoid of translation.[5,6,14,20,27,28] However, single-molecule analyses show that translating mRNAs are not forbidden inside of SGs,[29] and some report that translation inside of SGs might not be a rare event compared to translation in the cytosol.[30]

G3BPs, in addition to being required for formation of canonical SGs,[1,2] are also sufficient to nucleate SG assembly in the absence of stress, either by overexpression or by optogenetic manipulation.[31,32] These proteins also play roles in unstressed cells, including translational

upregulation of target mRNAs in fly cells and rescue of ribosomal subunits from lysosomal degradation.[21,23]

Despite their many connections to translation and the stress response, the overall impact that G3BPs and SGs have on translation during stress or, indeed, whether they have any impact on translation during stress is not fully understood.[14,33-35] Previous attempts to determine the effects of G3BPs or SGs on translation have relied either on bulk measurements of translation with limited sensitivity and specificity, such as S^{35} labeling of nascent peptides, or have been restricted to observations of single genes and reporters.[1,21,30] Here, we use spike-normalized ribosome profiling and optogenetic methods to measure the impact of G3BPs and SGs on translation with and without stress. These results support a model in which G3BPs and SGs reinforce the ISR translation program by prioritizing the translation of their most enriched transcripts.

RESULTS

Ribo-spike Enables Observation of Absolute Translation Changes during the ISR

A variety of cellular stresses induce the ISR, resulting in eif2α phosphorylation and a drastic global reduction in translation. Such global changes to translation have been challenging to observe by ribosome profiling because ribosome profiling typically reports the relative translation efficiencies (TEs) in each sample with no information on the absolute differences between samples.[36] In other high-throughput approaches, spiking known amounts of orthogonal standards into to each starting sample enables quantification of absolute differences. However, spiking in short RNAs resembling ribosome-protected fragments (RPFs) would not be appropriate for samples analyzed by ribosome profiling, as these samples are treated with RNAse to create RPFs, which would destroy the unprotected spike molecules. Normalizing to endogenous mitochondrial RPFs can bypass this problem.[36,37] However, an assumption underlying this approach is that mitochondrial translation is unaffected by the experimental condition—an assumption not always expected to be valid, especially if cells are subjected to stress.

To use ribosome profiling to measure absolute changes to TE occurring as a consequence of stress, we developed a ribosome profiling spike-in (ribo-spike) (Fig 1A). Firefly luciferase mRNA was translated in vitro, using a rabbit-reticulocyte translation system, and while the reaction was undergoing maximal translation, it was treated with cycloheximide to block ribosome translocation and flash frozen for storage. A defined amount of this reaction containing ribosomes translating the orthogonal firefly luciferase mRNA was then spiked into each sample as the ribo-spike. To confirm that these ribo-spikes functioned as intended, we added them in equal quantities to a dilution series of cellular lysates and performed ribosome profiling on these lysates. For both RPF and mRNA measurements, concentrations of the dilution series calculated based on the spike-ins closely matched the known dilutions (Fig S1A).

To apply the ribo-spike in the context of the ISR, we stressed cells with 500 µM sodium arsenite, which causes oxidative stress, for 1 h and compared them to unstressed cells using ribosome profiling with our ribo-spike. This dose of sodium arsenite activates the ISR, leading to eif2α phosphorylation and substantial global reduction in translation.[1,20] By normalizing to the spike-in TE across samples we were able to detect and measure absolute changes in TE for

mRNAs of >10,000 individual genes. Aggregating these measurements revealed a drastic (20-fold) global reduction in TE, consistent with previous bulk measurements (Fig 1B and S1B,C).[1,38,39] Interestingly, TEs of mitochondrial mRNAs increased in the presence of sodium arsenite (Fig 1B), validating our concern that the TEs of mitochondrial mRNAs might not remain constant under stress conditions.

Against the backdrop of a drastic global reduction of translation during stress, some mRNAs retained or even enhanced their translation in response to stress. Among them were mRNAs of several stress-responsive genes previously reported to maintain their translation during the ISR, including *ATF4*, *ATF5*, *CEBP*α, and *DDIT3*/*CHOP* (Fig 1B). Many of these mRNAs are known to contain upstream open reading frames (uORFs), which can help regulate their translation during stress.[40] Indeed, regulation by uORFs is proposed to help shape the general translation response to stress.[6,8,11,12,41,42] Supporting this proposal, among the mRNAs with retained or enhanced translation, we observed a strong bias in those reported to contain one or more functional uORF (Fig S1D).[43]

In yeast, newly transcribed mRNAs tend to be preferentially translated during stress.[44,45] To assess this possibility in mammalian cells, we compared the translation change in response to stress to mRNA half-lives, reasoning that mRNAs with short half-lives would be predominantly composed of newly synthesized transcripts. Consistent with the observations made in yeast, we observed a moderate negative correlation between the translation change of an mRNA upon stress and its estimated half-life (Fig S1E; $R_S = -0.22$).[46]

At the other extreme, some mRNAs were especially sensitive to the translation shutdown, including *CSDE1* and *PCBP2*, consistent with a previous study.[42] Interestingly, other hypersensitive mRNAs encoded proteins involved in energetically expensive processes, such as vesicle trafficking (*COPS3*, *COPS6*, *CLTC*, *SCFD1*), which are strongly down-regulated during stress (Fig 1B).[47]

To measure absolute TE changes in another stress context, we performed analogous experiments in cells exposed to 45°C heat shock (Fig 1C and S1B,C). The results resembled those observed for arsenite stress. First, normalizing to the ribo-spike again revealed a large reduction in global translation, although the median reduction of 8-fold was somewhat less than the 20-fold reduction caused by arsenite stress. Second, mitochondrially translated mRNAs again had higher TE in stressed cells, indicating that mitochondrial translation might generally be altered in the context of global cellular stress. Third, mRNAs with retained or enhanced TE again included those of previously identified stress-responsive, uORF-containing genes (*ATF4*, *ATF5*, *CEBP*α, *DDIT3*/*CHOP*, and *BiP*/*GPR78*), and short half-life transcripts (Fig 1C and S1F,G). Fourth, mRNAs hypersensitive to heat shock translation shut down again included *CSDE1*, *PCBP2*, and *CLTC*, as well as the mRNA for the vesicle trafficking gene *VSP4A* (Fig 1C). Despite this overlap and an overall correlation between the changes observed with these two different stressors (Spearman R, $R_S = 0.63$), the translation changes were not identical, and many genes were called as being differentially regulated in one stress but not the other (Fig S1H–J). This observation concurred with previous reports that the extent to which specific mRNAs are up- or downregulated can depend on the particular type and dosage of stress.[7]

We consider the combination of widespread translation shutdown, the retained or increased translation of select transcripts, and the hypersensitive downregulated translation of others to be the ISR translation program. The ability to observe these ISR translation programs

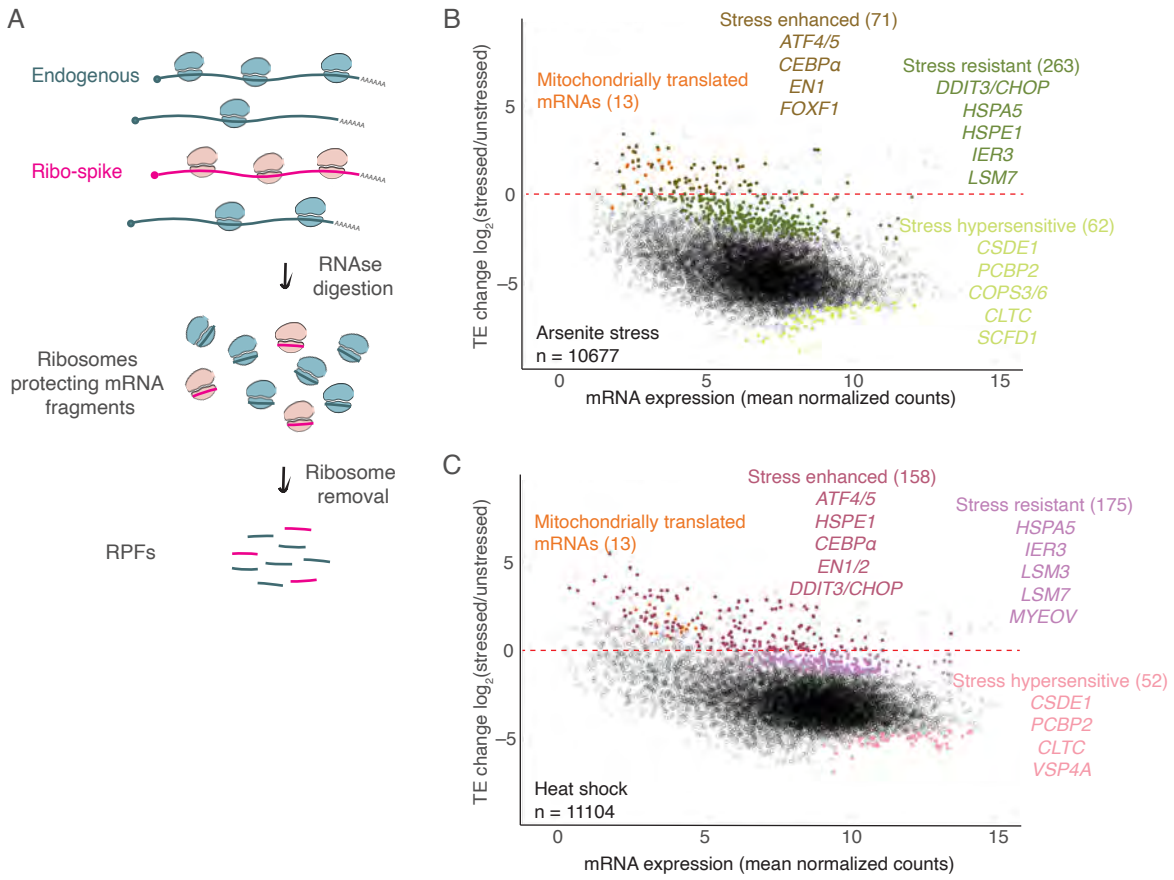

Figure 1. Ribo-spike enables observation of absolute translation changes during ISR. (A) Schematic representation of the ribo-spike. The ribo-spike consists of polysomes formed on an orthogonal mRNA sequence, in this case firefly luciferase mRNA (*fLuc*) translated in a rabbit reticulocyte lysate. A defined amount of the ribo-spike sample is added to each experimental sample, ultimately generating orthogonal RPFs that enable normalization between samples. **(B)** The ISR translation program induced upon arsenite stress. Plotted for each mRNA is the $\log_2$ fold-change (FC) in TE observed in HCT116 cells responding to 500 µM sodium arsenite (for 1 h) as a function of the mRNA expression. The red dashed line indicates unchanged TE, as determined by the ribo-spike. Points for stress-enhanced, stress-resistant, and stress-hypersensitive mRNAs are indicated by colors, with exemplar mRNAs listed for each category. Stress response categories were determined by DESeq2 ($\log_2$ FC > 1, adjusted p value < 0.05). Mitochondrially translated mRNAs are indicated in orange. n indicates number of unique mRNAs. **(C)** The ISR translation program induced upon heat shock (45°C for 25 min); otherwise, as in (A).

153 both under arsenite stress and heat shock illustrates how using ribo-spike enables accurate and
154 precise monitoring of absolute translation changes between samples and emphasizes the utility
155 of a truly orthogonal spike-in for studies monitoring global changes to translation.
156
157 **G3BPs Reinforce the ISR Translation Program**
158 Having developed a method to globally monitor absolute TE changes, we wanted to use it to
159 determine the effects of G3BPs and SGs on the cellular stress response. To do so, we also
160 needed to be able deplete cells of G3BPs and SGs. Therefore, we created a cell line in which

161 G3BPs could be inducibly depleted using an auxin-inducible degron (AID).[48,49] In HCT116 cells,
162 we tagged both alleles of both endogenous G3BP1 and endogenous G3BP2 with the AID and
163 RFP (AID::RFP::G3BPs). Adding indole-3-acetic acid (IAA, a form of auxin) induced rapid and
164 efficient depletion of both G3BPs, with approximately 90% of each protein being depleted
165 within 3 h, while imparting minimal effects on the stability of another SG-resident protein
166 PABPC1 (Fig 2A–C).
167 To determine whether our AID-mediated depletion of G3BPs was sufficient to prevent
168 formation of SGs, we labeled endogenous PABPC1, a canonical SG marker, with GFP and
169 assessed SG formation after subjecting cells to oxidative stress by treatment with sodium
170 arsenite. As expected, depletion of G3BPs prior to stress largely prevented formation of SGs, as
171 marked by PABPC1, with < 3% of cells still able to form visible SGs (Fig 2C,D). To examine if this
172 result was generalizable across different stresses, we repeated this experiment using heat shock
173 instead of arsenite stress. Under this different stress, results were similar, with < 5% of cells able
174 to form visible SGs (Fig 2E,F). These results were consistent with those of previous experiments
175 that use long-term knockdown or knockout of G3BPs to show that these proteins are necessary
176 nucleators of SG assembly.[1,2]
177 Having generated these degron lines, we set out to determine the impact of G3BPs and SGs
178 on translation during stress, using ribosome profiling with the ribo-spike to monitor translation
179 differences in cells subjected to arsenite stress either with or without prior depletion of G3BPs,
180 and thus with or without the ability to form SGs (Fig 2G). Compared to G3BP-depleted cells,
181 normal cells underwent a somewhat stronger inhibition of global translation (1.4-fold, Fig S2A).
182 This modest effect was consistent with reports that G3BP is largely dispensable for the global
183 reduction in translation caused by the ISR.[1]
184 Although the effect was relatively small, we were nonetheless intrigued to find that G3BPs
185 and perhaps SGs did seem to contribute, if only modestly, to the massive reduction in
186 translation that occurs during the ISR. To further examine this contribution of G3BPs and
187 potentially SGs to the ISR translation program, we compared the translation changes caused by
188 presence of G3BPs to those caused by activation of the ISR. We observed a clear positive
189 correlation (R_S = 0.33) between the mRNAs regulated by G3BPs and those regulated by the ISR
190 (Fig 2H and S2B). This implied that G3BPs, and perhaps SGs, tend to upregulate the same
191 mRNAs that the ISR upregulates and tend to downregulate the same mRNAs that the ISR
192 downregulates, thereby reinforcing the ISR translation program.
193 Given that the ISR translation program for arsenite-treated cells and heat-shocked cells were
194 distinct, we examined whether G3BPs also reinforced the heat shock ISR translation program.
195 When comparing the G3BP-dependent translational changes observed during heat shock to the
196 heat-shock-induced ISR translation changes, the results resembled those observed for arsenite
197 stress. Although the G3BP-dependent reduction to translation was negligible, especially when
198 compared to the much larger reduction caused by the ISR (1.06- and 8-fold, respectively; Fig 1C
199 and S2C), we again observed a positive correlation (R_S = 0.43) between changes of mRNAs
200 regulated by G3BPs and those regulated by the ISR (Fig 2J and S2D). Taken together, these
201 results indicated that G3BPs, and perhaps SGs, reinforce the ISR translation program across
202 multiple stresses.
203 To examine whether the factors we observed impacting mRNA translation during stress
204 (presence of uORFs and short half-life) also impacted the effect of G3BP on translation, we

compared both uORF presence and estimated mRNA half-lives to G3BP-dependent translation in cells treated with arsenite or heat shock. We observed that mRNAs containing one or more functional uORF were preferentially translated in the presence of heat stress. However this trend did not hold in arsenite-stressed cells (Fig S2E,F), indicating that, although uORFs may play a role in G3BP-dependent translation during stress, it appears to be a minor or stress-specific role. Furthermore, we observed no correlation between the half-life of an mRNA and its G3BP-dependent translation (Fig S2G,H), indicating that, although newly synthesized mRNAs might be translationally favored, their regulation appears to be stress-granule independent.

To determine whether the G3BP-dependent translation effects that we observed were a constitutive or stress-specific function of G3BPs— potentially through formation of SGs, we performed identical ribosome profiling experiments, comparing cells containing G3BPs to cells depleted for G3BPs but this time in the absence of stress. This allowed us to quantify transcriptome-wide G3BP-dependent translation changes in the absence of stress. When comparing G3BP-dependent translation changes in unstressed cells to the changes caused by activation of the ISR, unstressed G3BP-dependent translation changes had no positive correlation to the translation changes of either the arsenite-induced ISR or the heat-shock-induced ISR (R_S = –0.033 and –0.12 respectively; Fig 2I, K). Together these results argued that G3BPs reinforce the ISR translation program in a stress-dependent manner and were consistent with a model in which this is a function of G3BP through its nucleation of SGs.

Because G3BPs are required for SG formation, we could not say whether the effects we observed upon depleting G3BPs were a consequence of losing SGs or whether they were a consequence of losing some other G3BP function. We sought to disambiguate G3BP and SG function by targeting CAPRIN1 or UBAP2L, two other proteins reported to be required for SG formation,[1,19,50,51] reasoning that observing the same effects when SGs were depleted by removing a different protein would support the idea that the effects were a consequence of removing SGs. We first targeted CAPRIN1, a G3BP interactor that colocalizes to SGs, using the AID system and assessed SG formation by following G3BP and eIF4G localization. No reduction in SG formation was detected (Fig S2I – M). We then targeted UBAP2L, another SG-localized protein, and assessed granule formation by following PABPC1 localization. Again, no significant reduction in SG formation was detected (Fig S2N – Q). These results concurred with findings that in many cell types G3BPs are uniquely required for SG formation and illustrated the difficulties in genetically disentangling the functions of SGs from those of their required G3BP components.[2]

SGs are Enriched for mRNAs that are Favored by the ISR Translation Program

After difficulty using this genetic approach to define the role of SGs, we turned to other approaches. One attractive hypothesis was that mRNAs that are differentially regulated by the ISR translation program are also differentially localized to SGs and that this localization to SGs determines the effect that G3BPs have on translation of those mRNAs during stress. To assess the relationships between regulation by the ISR translation program, regulation by G3BPs, and SG localization, we purified stress granule cores. Using an established protocol,[18,52] cores were purified from HCT116 cells treated with 500 µM sodium arsenite for one hour, and both the SG-associated and total-cytoplasmic transcripts were sequenced. Analysis of these datasets identified 488 transcripts that were significantly enriched in SG cores and 453 that were

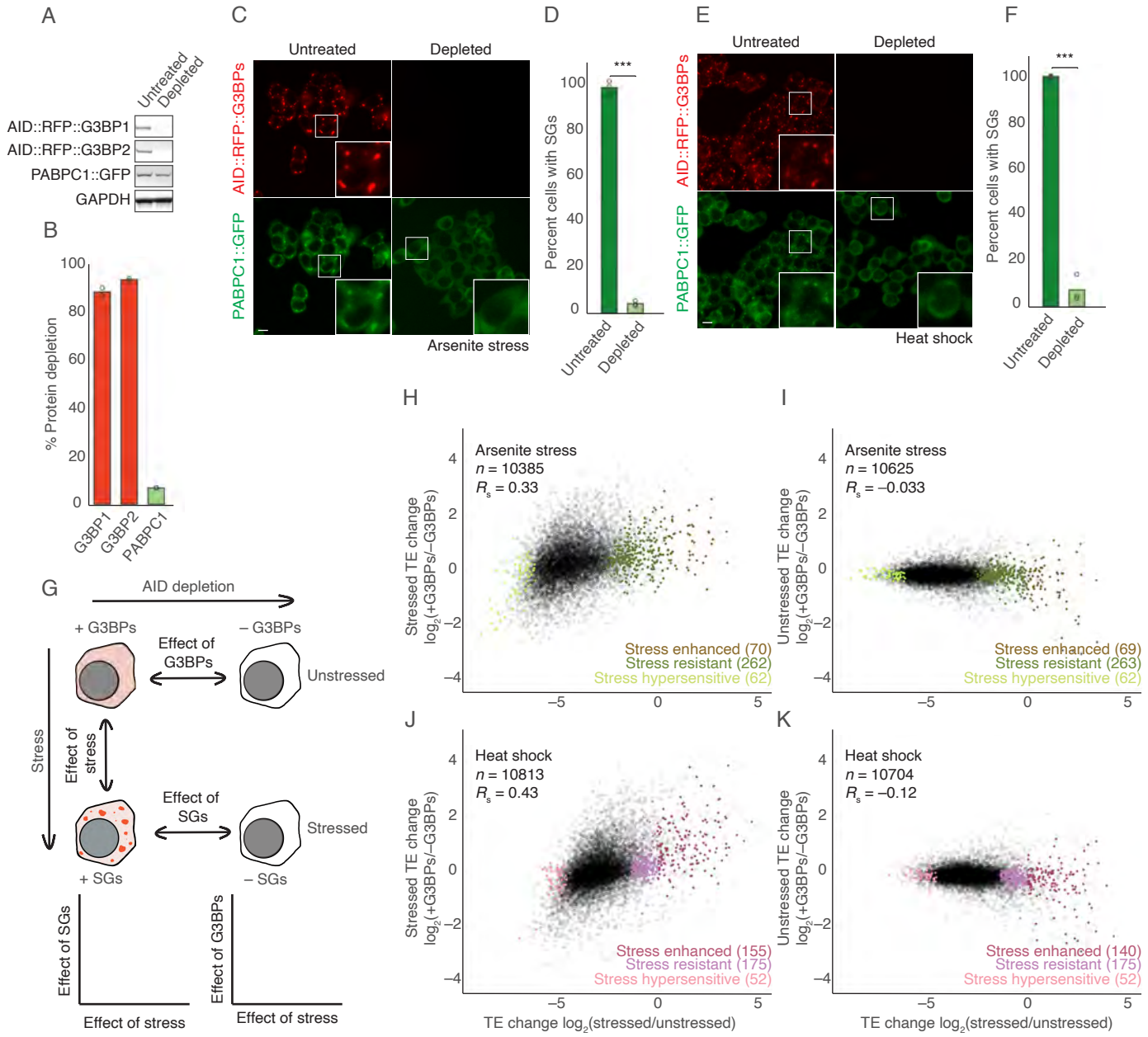

Figure 2. G3BPs reinforce the ISR translation program. (A) Depletion of endogenous G3BPs fused to AID. Immunoblots probed for the indicated proteins show specific depletion of AID fusion proteins after treatment with 500 µM IAA for 3 h. **(B)** Quantification of protein depletion in (A), normalizing to levels of GAPDH. Points show values for two biological replicates. **(C)** Prevention of SG formation during arsenite stress. HCT116 cells were either treated with 500 µM IAA to deplete G3BPs (right) or not treated (left) prior to arsenite stress (500 µM sodium arsenite for 1 h). Images show either G3BPs in red or SG marker protein PABPC1 in green (scale bar, 10 µm). **(D)** Quantification of SG formation in (C). Points show values for three biological replicates (***, $p \leq 0.001$; Welch's two-sample t-test). **(E, F)** Prevention of SG formation during heat shock (45°C for 25 min); otherwise, as in (C, D). **(G)** Schematic representation of G3BP-depletion experiment. Ribosome profiling was performed on stressed HCT116 cells to determine the effects of stress on translation, G3BP-depleted unstressed HCT116 cells to determine the effect of G3BPs on translation, and G3BP-depleted stressed HCT116 cells to determine the effects of G3BPs/SGs on translation. The effects of stress were then compared to the effects of G3BPs and SGs. **(H)** Relationship between G3BP-dependent translation during arsenite stress and the ISR translation

(H) Relationship between G3BP-dependent translation during arsenite stress and the ISR translation program. The plots indicate the $\log_2$ FC in TE due to presence of G3BPs in cells treated with arsenite as a function of the $\log_2$ FC in TE due to arsenite. Points for stress-enhanced, stress-resistant, and stress-hypersensitive mRNAs are indicated by colors. *n* indicates number of unique mRNAs. **(I)** Relationship between G3BP-dependent translation in the absence of stress and the ISR translation program; otherwise, as in (H). **(J)** Relationship between G3BP-dependent translation during heat shock and the heat-shock ISR translation program; otherwise, as in (H). **(K)** Relationship between G3BP-dependent translation in the absence of stress and the ISR translation program; otherwise, as in (H).

250
251 significantly depleted (Fig 3A, >2-fold change, adjusted *p* value <0.05).
252 Overall, our SG enrichments observed in HCT116 cells resembled those previously observed
253 in U2OS cells (Fig S3A, R_S = 0.50),[18] especially when considering the differences between the
254 two cell types, as reflected in their overall total-mRNA expression profiles (Fig S3B, R_S = 0.66).
255 Moreover, as found in U2OS cells,[18] longer mRNAs and mRNAs that were poorly translated prior
256 to stress tended to be enriched in SGs purified from HCT116 cells (Fig S3C,D). These similarities
257 with the results previously obtained with U2OS cells indicated that we had successfully purified
258 SG cores.
259 We next examined the relationship between differential regulation by the ISR translation
260 program and SG localization and found that mRNAs that retained or improved their translation
261 during stress tended to be more enriched in SGs, whereas mRNAs that were especially sensitive
262 to translation shutdown tended to be depleted (Fig 3B). To evaluate whether this relationship
263 was simply a consequence of SGs being enriched for transcripts that were poorly translated
264 prior to stress, which might have experienced a smaller decline upon translation shutdown, we
265 also examined the relationship between TE during stress and SG enrichment and found that SGs
266 were enriched for mRNAs that were translated relatively well during stress (Fig S3E).
267 Furthermore, analyses of published measurements of SG-enrichment in U2OS cells treated with
268 sodium arsenite[18], stress-dependent RNA-granule enrichment in NIH 3T3 cells treated with the
269 potent ER stressor thapsigargin [53], and stress-dependent G3BP proximity labeling in HEK293T
270 cells treated with sodium arsenite[54] yielded similar, albeit sometimes weaker, trends (Fig S3F –
271 J). Together, these results supported a model in which mRNAs that are favored by the ISR
272 translation response preferentially localize to SGs and suggest that this model might be
273 generalizable across multiple stresses and cell types.
274
275 **SG-Enriched mRNAs are Favored by G3BPs During Stress**
276 To assess whether SG localization might influence regulation by G3BPs during stress, we
277 examined the relationship between G3BP dependence of translation during arsenite treatment
278 and SG enrichment. Surprisingly, mRNAs enriched in SGs of our HCT116 cells tended to have
279 higher TE in the presence of G3BPs during stress, whereas mRNAs depleted from SGs tended to
280 be translationally repressed in the presence of G3BPs during stress (Fig 3C). Repeating this
281 analysis with SG enrichment data from arsenite-treated U2OS cells[18] yielded similar but weaker
282 relationships (Fig S3K). Likewise, an analysis comparing our G3BP-dependent translation during
283 heat shock to previous measurements of stress-dependent RNA-granule enrichment in heat-
284 shocked NIH 3T3 cells[53] showed that mRNAs targeted to the SG-enriched fraction tended to
285 have higher TEs in the presence of G3BPs (Fig S3L). Moreover, comparison of our G3BP-

286 dependent translation during arsenite stress to SG-enrichment in arsenite-stressed HEK293T
287 cells previously measured by proximity labeling[54] yielded analogous results (Fig S3M). Thus, in a
288 variety of stress and cell-type contexts, the G3BPs favor the translation of SG-enriched mRNAs
289 or inhibit the translation of SG-depleted mRNAs. Taken together, the results of our SG-
290 purification experiments suggested a model in which those transcripts that are most strongly
291 upregulated by the ISR translation program localize to SGs, leading to further upregulation by
292 G3BPs.
293

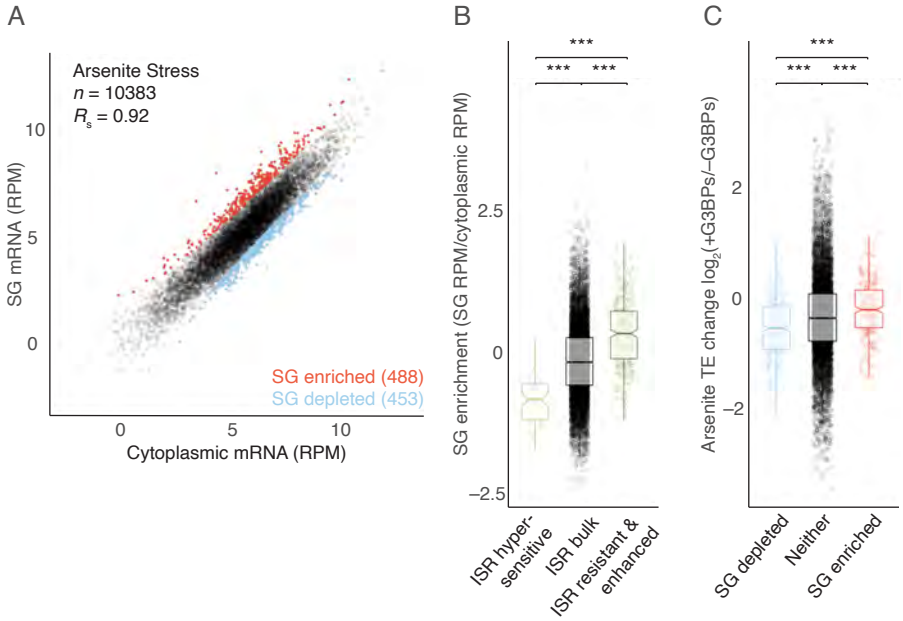

Figure 3. Translation of SG-enriched mRNAs is favored by G3BPs. (A) mRNAs enriched and depleted in SGs. Plotted for each mRNA is its abundance in the SG fraction as a function of its abundance in the cytoplasmic fraction. Points for SG-enriched and SG-depleted mRNAs, as determined by DESeq2 ($\log_2$ FC > 1, adjusted p value < 0.05), are indicated in red and blue, respectively, with their numbers in parentheses. n indicates total number of unique mRNAs. **(B)** Relationship between SG enrichment and ISR translation. Plotted are the SG enrichments of mRNAs in each of three ISR translation categories: stress-enhanced/resistant, bulk behavior, and stress-hypersensitive (line, median; notch, 95% confidence interval; box, quartiles; whiskers, 1.5 x IQR); ***, $p \leq 0.001$; Welch's two-sample t-test). **(C)** Relationship between G3BP-dependent translation and SG enrichment. The plots indicate the $\log_2$ FC in TE due to presence of G3BPs in stressed cells for mRNAs in each of three SG-enrichment categories: SG-enriched, SG-depleted, and neither; otherwise as in (B). All stresses were 500 µM sodium arsenite for 1 h.

294 **SG-like OptoGranules Drive Global Reduction in Translation without a Full ISR**
295 Our global analyses of the effects of G3BPs on translation showed that G3BPs, while not
296 required to establish the ISR translation program, do reinforce it. To determine whether
297 formation of SGs was responsible for these additional changes to translation during the ISR and
298 whether SGs were indeed sufficient to drive these translation changes in the absence of
299 exogenous stress, we set out to find a system in which we could form ectopic SGs and assess
300 their effect on translation in the absence of exogenous stress.
301 Ubiquitin-associated protein 2-like (UBAP2L) is reported to be sufficient to drive ectopic SG
302 formation in the absence of exogenous stress.[55] Accordingly, in an attempt to nucleate ectopic
303 SG formation, we used the PiggyBac system to integrate multiple copies of doxycycline-

304 inducible, RFP-tagged UBAP2L (RFP::UBAP2L) into HCT116 cells. As expected, doxycycline
305 induction caused UBAP2L puncta to form in most cells. However, these puncta were smaller and
306 more numerous than typical SGs, and did not colocalize with the canonical SG marker eIF4G,
307 which indicated that they were not authentic SGs (Fig S4A,B).
308 Overexpression of G3BP1 is also reported to be sufficient to drive ectopic SG formation in
309 the absence of exogenous stress.[31] When we overexpressed GFP-tagged G3BP1 using the
310 PiggyBac system, G3BP puncta formed with similar size and morphology as stress granules.
311 Moreover, these puncta were positive for the canonical SG marker, eIF4G, as expected if these
312 puncta were authentic SGs. However, these SGs formed in only ~20% of cells overexpressing
313 G3BP1 (Fig S4C,D).
314 To form ectopic SGs in a higher fraction of cells, we turned to the CRY2 optogenetic system,
315 in which the light-dependent cryptochrome 2 (CRY2) photolyase homology region (PHR)
316 oligomerization domain (hereafter referred to simply as CRY2) is fused to G3BP1, enabling
317 spontaneous SG-like condensates to be nucleated in response to blue light.[32] These
318 OptoGranules contain many known markers for authentic SGs.[32] In our adaptation of this
319 method, we removed the NTF2L domain at the N-terminus of G3BP1 and replaced it with the
320 CRY2 domain tagged with GFP (GFP::CRY2::G3BP$_{\Delta N}$) (Fig 4A). This construct was placed under a
321 doxycycline-inducible promoter and integrated into cells using the PiggyBac system. Even in the
322 absence of blue light, inducing the expression of GFP::CRY2::G3BP$_{\Delta N}$ caused formation of
323 ectopic puncta in ~20% of cells, which resembled the percentage observed when
324 overexpressing GFP::G3BP1. Nevertheless, exposing these cells to 488 nm blue light from an
325 LED array enhanced puncta formation, such that they were observed in ~80% of cells within 3 h.
326 Removal of the blue light caused disassembly of puncta, reaching the basal 20% of cells within 2
327 h, which showed that for most, if not all, of the granules, formation was reversible (Fig 4A, S4E).
328 We next examined whether these granules had SG markers and behavior. Consistent with
329 previous findings,[32] our light-induced granules were positive for canonical SG markers eIF4G and
330 CAPRIN1 (Fig 4B and S4F). FRAP experiments showed that these granules recovered from
331 photobleaching on a time scale similar to that of canonical SGs, indicating that these granules
332 shared similar dynamics (Fig S4G). Together, these results showed that our OptoGranules (OGs)
333 were dynamic, reversible, SG-like condensates formed in the absence of exogenous stress.
334 To determine whether formation of these OGs was sufficient to drive translation changes
335 even in the absence of exogenous stress, cells expressing GFP::CRY2::G3BP$_{\Delta N}$ were exposed to
336 blue light for three hours, allowing OGs to form in most cells, and then subjected to ribosome
337 profiling using our ribo-spike. To control for the effects of exposing cells to blue light, ribosome
338 profiling was also performed on cells that were exposed to blue light but were not induced to
339 express GFP::CRY2::G3BP$_{\Delta N}$ and therefore formed no OGs.
340 If formation of OGs were sufficient to drive ISR-like translation changes, then we would
341 predict that analysis of our ribosome-profiling data would yield the following results. First, as
342 with the ISR translation program, cells with OGs would be predicted to undergo a global
343 reduction in TE compared to cells only exposed to blue light. Second, these translation changes
344 would be predicted to positively correlate with those observed in the ISR, with similar genes
345 retaining their translation in the face of widespread decreases in TE, and with similar genes
346 being especially sensitive to that translation shutdown. Third, OG-induced translation changes
347 would be predicted to correlate positively with the G3BP-dependent translation during stress.

348 Fourth, transcripts enriched in SGs would be predicted to also be resistant to any translation
349 shutdown caused by the formation of these SG-like condensates.
350 When TEs in OG-induced cells were compared to those in blue-light controls, a global
351 reduction in translation was observed. This reduction was modest (1.6-fold) compared to the
352 drops in translation caused by the ISR translation program (20-fold for 1 h of 500 µM sodium
353 arsenite stress and 8-fold for 25 min of 45°C heat shock) (Fig 4C). This modest reduction was
354 consistent with the results of the AID-depletion experiments that indicted that G3BPs, which are
355 essential for SG formation, were responsible for only a small fraction of the translation
356 shutdown observed during the ISR.
357 Although this observation was consistent with the first of our four predictions, analyses of
358 the TE results failed to confirm any of the other three predictions regarding the effects of OG
359 induction on translation. OG translation changes did not correlate with either the ISR translation
360 program or G3BP-dependent translation changes in stressed cells (Fig 4D,E, R_S = 0.019 and –
361 0.054, respectively). Additionally, although mRNAs depleted in SGs tended to be more sensitive
362 to the translation shutdown caused by formation of OGs, mRNAs that were enriched in SGs did
363 not perform any better than those that were neither enriched nor depleted (Fig 4F). Considered
364 together, these results argued that spontaneous formation of the SG-like OGs, while sufficient
365 to drive a modest reduction in global translation, was not sufficient to specify the ISR translation
366 program.
367
368 **OptoGranules Require Cellular Stress to Recruit an SG Transcriptome**
369 One caveat of our predictions of TE changes that might be observed upon OG formation was
370 that we assumed that the spontaneously formed OGs contained the same transcriptome as SGs
371 and therefore would have the opportunity to regulate those transcripts in the same manner.
372 This assumption is consistent with the recent proposal that G3BP is the central scaffold of a
373 complex protein-RNA interaction network. According to this model, G3BPs nucleate SG
374 formation by switching to a higher valency conformation when triggered by increased levels of
375 free cytosolic RNA.[2-4] This model suggests that simply increasing the valency of G3BPs, as in the
376 case of the CRY2 system, might be sufficient to establish that same complex interaction
377 network, even in the absence of stress. Interestingly, this prediction is also consistent with the
378 observation that the established determinants of the SG transcriptome (transcript length and TE
379 prior to stress) are parameters that are independent of stress and is further supported by the
380 observation that OGs are positive for many canonical SG markers (Fig S4E).[18,32] However,
381 prominent paradigms of SG formation state that the SG transcriptome is largely determined by
382 the transcriptome RNA-binding landscape (the landscape created by proteins bound to the
383 transcriptome), meaning that mRNAs that are most available to self-associate or be stably
384 bound by SG assembly factors and remodeled into messenger ribonucleoprotein (mRNP)
385 complexes are the most likely to be incorporated into SGs.[2,14,56,57] Indeed, stress can
386 dramatically shift the RNA content of other biological condensates such as P-bodies and P
387 granules.[58,59] Thus, because cellular stress dramatically remodels the RNA-binding landscape,
388 SGs formed in the presence of stress and OGs formed in the absence of stress might recruit
389 different sets of mRNAs, despite their general compositional, morphological, and biophysical
390 similarities.
391

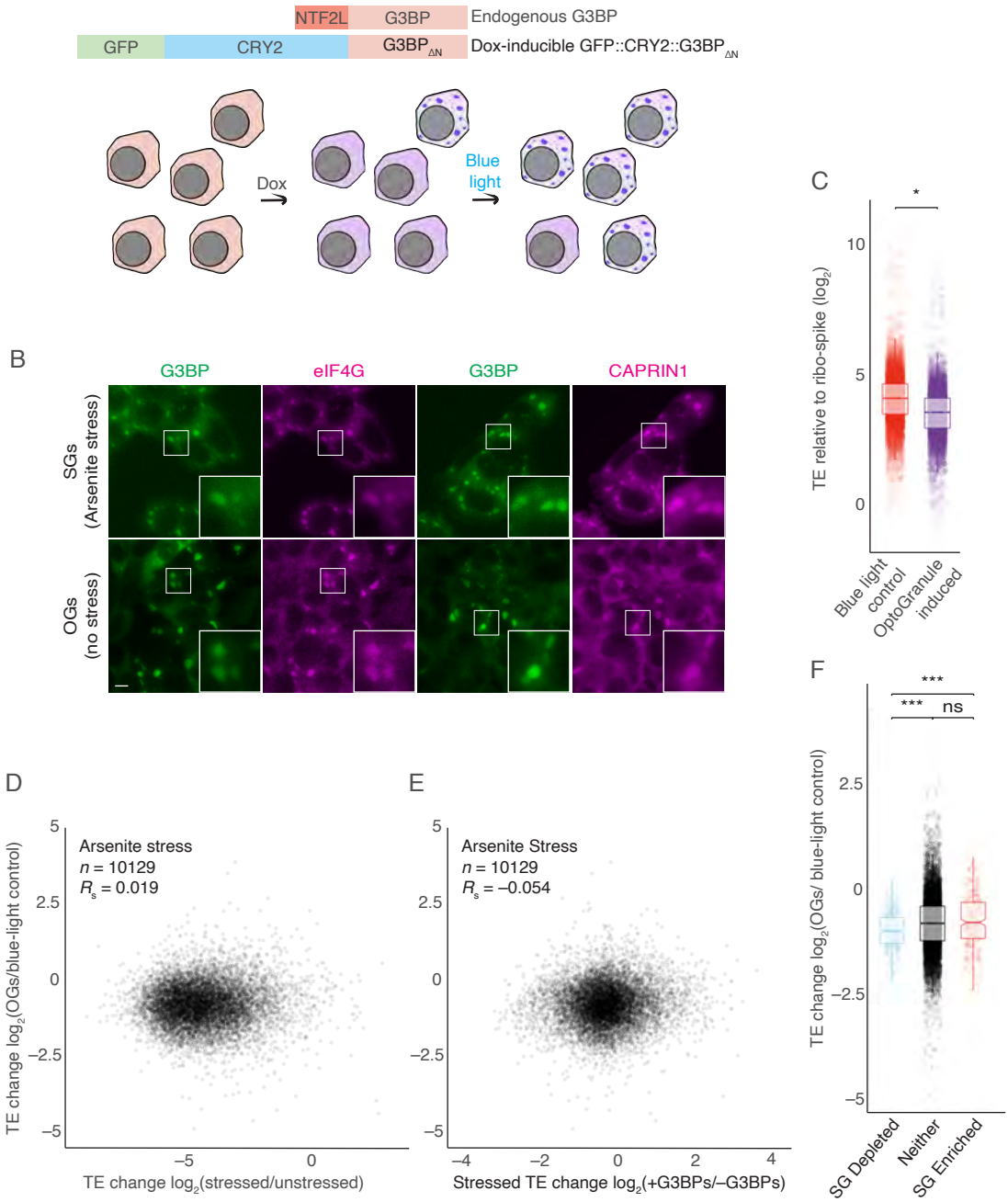

Figure 4. SG-like OGs Can Drive a Global Reduction in Translation. (A) Schematic representation of the OG system. HCT116 cells expressing endogenous G3BP containing an NTF2L dimerization domain were edited to also express doxycycline (dox)-inducible ectopic G3BP in which the NTF2L domain had been replaced with a fusion of GFP and the light-inducible CRY2 dimerization domain (GFP::CRY2::G3BP$_{\Delta N}$). After doxycycline induction, a minority of cells formed ectopic granules. After exposure to blue light (488 nm), most cells formed ectopic granules. **(B)** SG marker localization to OGs. HCT116 cells expressing wild-type GFP::G3BP1 were either stressed with 500 µM sodium arsenite for 1 h (top) or treated with 1 µM doxycycline to induce expression of GFP::CRY2::G3BP$_{\Delta N}$ and exposed to blue light for 3 h (bottom). Fluorescent or immunostained proteins are as indicated (scale bars, 10 µm). White boxes highlight insets that are expanded on the right.

392

(C) Comparison of TE in OG-induced cells to that in blue-light control cells. Plotted are the TE distributions in HCT116 cells in which GFP::CRY2::G3BP$_{\Delta N}$ was expressed and exposed to blue light to form OGs (right) and in control cells expressing only wild-type G3BP exposed to blue light, in which no OGs were formed (left) (line, median; notch, 95% confidence interval; box, quartiles; whiskers, 1.5 x IQR). Significance was determined using ribo-spike values as in Figure S1B (*, $p \leq 0.05$; Welch's two-sample t-test). **(D)** Comparison of OG and ISR translation programs. Plotted is TE change caused by induction of OGs as a function of TE change caused by arsenite. *n* indicates total number of unique mRNAs. **(E)** Comparison of OG and G3BP-dependent translation programs. Plotted is TE change caused by OGs as a function of TE change caused by presence of G3BPs in arsenite-treated cells; otherwise, as in (C). **(F)** Comparison of OG translation program and SG enrichment. The plots indicate the $\log_2$ FC in TE caused by induction of OGs for mRNAs in each of three SG enrichment categories: SG-enriched, SG-depleted, and neither (line, median; notch, 95% confidence interval; box, quartiles; whiskers, 1.5 x IQR); ns, not significant; ***, $p \leq 0.001$; Welch's two-sample t-test).

To test this hypothesis, we set out to purify OGs formed in either the absence or the presence of stress. To purify OGs formed in the absence of stress, we used the same approach as in our previous ribosome-profiling experiment. To purify OGs formed in the presence of stress, we combined our OG and AID systems. We integrated the doxycycline-inducible GFP::CRY2::G3BP$_{\Delta N}$ construct into cells expressing endogenously edited AID::RFP::G3BPs and doxycycline-inducible OsTIR1, the E3 ligase responsible for the turnover of the AID. Upon treatment with doxycycline and IAA, these cells degraded their endogenous G3BPs and replaced them with GFP::CRY2::G3BP$_{\Delta N}$, which rendered them incapable of forming SGs in the absence of blue light, even when treated with 500 µM sodium arsenite for 1 h. However, when these stressed cells were exposed to blue light, they readily formed granules (Fig 5A,B). We refer to these OGs formed in the presence of stress as StressOptoGranules (SOGs).

We then purified and sequenced the transcripts associated with both OGs and SOGs. As controls, we also examined real SGs purified from each cell line, i.e., from the OG line subjected to stress in the absence of blue light, and from the SOG line subjected to stress in the absence of both IAA and blue light (Fig 5C,D). We then examined all pairwise comparisons of granule enrichments, including our original SG enrichment data acquired from the parental line as an additional control. When we compared across control SGs we saw that results for all of our controls were similar to each other, with R_S values ranging from 0.72–0.75 (Fig 5E, Fig 5SA). However, when comparing results of control SGs to those of OGs formed in the absence of stress, substantially weaker correlation was observed, with R_S values ranging from 0.35–0.45 (Fig 5E, Fig 5SA). To determine if this difference was due to lack of cellular stress as opposed to some intrinsic bias of OG formation, we compared results of our control SGs to those of SOGs formed in the presence of stress. We found that transcripts enriched in SOGs were much more similar, and in fact nearly indistinguishable from those in SG controls, with R_S values ranging from 0.69–0.70 (Fig 5E, Fig 5SA). These differences in granule composition were not driven by differences in gene expression, as the cytoplasmic mRNA levels correlated quite well between these groups, with R_S values ranging from 0.84–0.96 (Fig 5F, Fig 5SB). Taken together, our results indicated that establishing the SG transcriptome requires not only the interaction network established by high valency G3BPs but also the RNA-binding landscape established during cellular stress.

Equipped with data on the enrichments within OGs, we were able to re-evaluate our prediction that granule-enriched transcripts would have favored translation during OG

formation. As expected, transcripts enriched in OGs better retained their translation, whereas transcripts that were depleted from OGs were most sensitive to the OG-induced translation shutdown (Fig 5G). This observation was consistent with a model in which enrichment in SGs favors translation, while depletion from SGs favors repression. Taken together, our OG ribosome-profiling and purification results supported a model in which SGs are sufficient to drive a modest decrease in global translation and to prioritize the translation of their enriched mRNAs while downregulating translation of mRNAs for which they are depleted. However, SGs require stress to induce an ISR-like translation program, presumably because the sorting of SG mRNAs is dictated by the cellular RNA-binding landscape, which is drastically remodeled upon activation of the ISR.

Tethering to SGs Imparts Resistance to ISR Translation Shutdown

Our findings suggested that localization to an SG grants an mRNA prioritized translation during the ISR translation shutdown, allowing the mRNA to better retain its TE. To test this model, we examined whether tethering reporters to SGs influenced their translation. The reporters each encoded nanoluciferase (nLuc) fused to the *E. coli* dihydrofolate reductase (ecDHFR) destabilizing domain, which causes rapid turnover of its protein fusions, ensuring reporting on recently translated nLuc.[60] The 3'UTR of each reporter mRNA also included an array of 24 bacteriophage MS2 hairpins, which bind MS2 coat protein (MCP).[30,61]

G3BPs strongly partition into SGs[1,31,62], and we found that in HCT116 cells almost half of our endogenous G3BP1 fusion protein (45.9%) was inside of SGs after 90 minutes of arsenite stress, a fraction that exceeded estimates in other cell lines (Fig S6A,B).[62] Considering this high partitioning coefficient, we chose endogenous G3BP1 as our SG-tethering protein. Using the PiggyBac system, reporters were stably integrated into HCT116 cells in which all endogenous G3BP1 alleles were tagged with either GFP (GFP::G3BP1) or MCP and GFP (MCP::GFP::G3BP1) (Fig 6A). We also explored the λN–BoxB aptamer system for tethering reporters to G3BP,[63,64] but in contrast to our results when expressing MCP::GFP::G3BP (Fig S6C), we observed perturbed G3BP localization and SG formation in cells expressing λN::GFP::G3BP.

To assess the effects of SG tethering for a variety of 5' and 3' UTRs, we created four different reporters using 5' and 3' UTRs from four mRNAs that had diverse behaviors in response to stress and to G3BPs, as measured by ribosome profiling (Table S1). Single-molecule fluorescence in situ hybridization (smFISH) with probes targeting the *nLuc* sequence indicated that the reporters were recruited to SGs at a basal level in cells expressing only GFP::G3BP, with an average of 30% of molecules localized to SGs across the four reporters (Fig 6B – D). In cells expressing MCP::GFP::G3BP, the reporters were more robustly recruited to SGs, with an average of 85% of reporter molecules localized to SGs (Fig 6B – D), which was a higher fraction recruited to SGs than that observed for 99% of endogenous mRNAs.[18]

Next, we measured how the translation of these reporters responded to arsenite stress. Cells were treated with 500 µM sodium arsenite for 90 min, and changes to protein production were monitored by measuring luciferase signal from these cells compared to that from unstressed control cells, and normalizing to total-protein levels. In addition, changes to mRNA levels were monitored by reverse transcription and quantitative PCR (RT-qPCR). Using these changes in translation and mRNA, changes in TE were calculated for each reporter. For untethered reporters, large decreases in TE were observed upon induction of stress, with a 25-

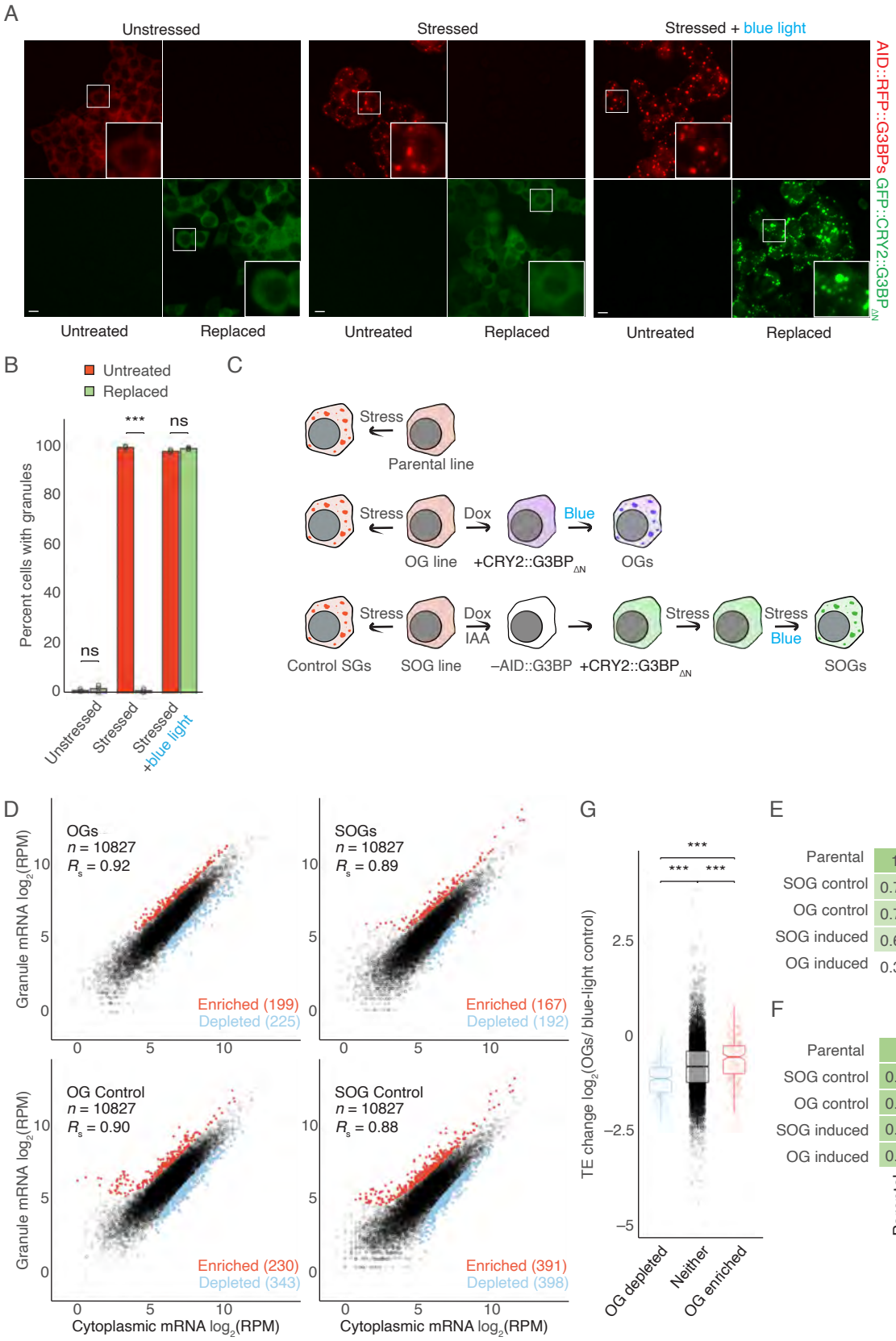
A
Unstressed
Stressed
Stressed + blue light
AID::RFP::G3BPs GFP::CRY2::G3BP$_{\Delta N}$
Untreated
Replaced
B
Untreated
Replaced
Percent cells with granules
***
ns
Unstressed
Stressed
Stressed +blue light
C
Stress
Parental line
Dox
Blue
OG line
+CRY2::G3BP$_{\Delta N}$
OGs
IAA
Control SGs
SOG line
–AID::G3BP
SOGs
D
OGs
n = 10827
R_s = 0.92
Enriched (199)
Depleted (225)
SOGs
n = 10827
R_s = 0.89
Enriched (167)
Depleted (192)
OG Control
n = 10827
R_s = 0.90
Enriched (230)
Depleted (343)
SOG Control
n = 10827
R_s = 0.88
Enriched (391)
Depleted (398)
Granule mRNA log$_2$(RPM)
Cytoplasmic mRNA log$_2$(RPM)
G
TE change log$_2$(OGs/ blue-light control)
OG depleted
Neither
OG enriched
E
SG mRNAs
Parental 1
SOG control 0.75 1
OG control 0.75 0.72 1
SOG induced 0.69 0.70 0.69 1
OG induced 0.35 0.38 0.45 0.46 1
F
Cytoplasmic mRNAs
Parental 1
SOG control 0.96 1
OG control 0.92 0.91 1
SOG induced 0.90 0.91 0.92 1
OG induced 0.86 0.84 0.93 0.87 1
Parental
SOG control
OG control
SOG induced
OG induced

469
470

Figure 5. OGs require stress to recruit the SG transcriptome. (A) Replacement of G3BP with GFP::CRY2::G3BP$_{\Delta N}$ to induce SOGs. In the left panel, HCT116 cells expressing endogenously tagged AID::RFP::G3BPs were either untreated (left) or treated with 1 µM doxycycline and 500 µM IAA for 18 h (right), leading to turnover of endogenous G3BP shown in red and expression of GFP::CRY2::G3BP$_{\Delta N}$ shown in green. In the middle panel, cells were treated as in left panel, but were subsequently stressed with 500 µM sodium arsenite for 1 h in the absence of blue light. In the right panel, cells were treated as in the middle panel, but were also exposed to blue light, beginning 30 min after start of the arsenite treatment (scale bars, 10 µm). White boxes highlight insets that are expanded on the right. **(B)** Quantification of granule formation in (A). Error bars report standard deviation for three biological replicates (*** $p \leq 0.001$, ns, not significant, Welch's two-sample t-test). **(C)** Schematic representation of granule purification experiment. Three cell lines were used: the parental HCT116 line expressing endogenous G3BPs, an OG HCT116 line expressing endogenous G3BPs and doxycycline-inducible GFP::CRY2::G3BP$_{\Delta N}$, and an SOG line expressing endogenous G3BP fused to AID and RFP (RFP::AID::G3BP), doxycycline-inducible OsTIR1, and doxycycline-inducible GFP::CRY2::G3BP$_{\Delta N}$. Control SGs were purified from each cell line by treating them with 500 µM sodium arsenite for 1 h. Additionally, OGs were purified from the OG line treated with doxycycline for 18 h, followed by 3 h of blue light, and SOGs were purified from the SOG line treated with both doxycycline and IAA for 18 h followed by exposure to arsenite stress for 30 min in the absence of blue light and then an additional 30 min of stress in the presence of blue light. **(D)** mRNAs enriched and depleted in the indicated types of granules; otherwise, as in Fig. 3A. **(E)** Comparisons of granule enrichments. The heatmap depicts the pairwise correlations (R_S values) observed between the enrichments of granules from (Fig. 3A and 5D). **(F)** Comparisons of cytoplasmic transcriptomes of cells used to determine granule enrichments (E). **(G)** Comparison of OG-dependent translation and OG enrichment. Plotted are distributions of TE changes caused by induction of OGs for mRNAs in each of three OG enrichment categories; otherwise, as in Fig 4E.

fold average drop in TE observed across the four reporters (Fig 6E,F). This drop was consistent with that expected for the translation of an mRNA during the ISR. Indeed, it aligned closely with the 20-fold average decrease in TE observed by ribosome profiling, indicating that our assay accurately reported on typical translation changes observed during stress. However, this uniform drop in translation also indicated that several of our reporters did not behave like their endogenous counterparts, some of which continue to be efficiently translated under stress conditions (Table S1), which implied that the 5' and 3' UTRs of these mRNAs were not sufficient to impart their endogenous translation responses to stress.

We proceeded to examine what happens to the translation of these reporters when tethered to SGs in the MCP::GFP::G3BP1 cell line. When tethered to SGs, each of our four reporters retained its translation significantly better than when untethered, with an average drop in TE of 2-fold when tethered, compared to 25-fold when untethered (Fig 6E,F). To control for the possibility that this might have been the result of recruiting a generic protein to the 3' UTRs of the reporters, we repeated the experiment in the untethered GFP::G3BP cell lines but this time also expressing MCP::BFP at levels similar to those of MCP::GFP::G3BP (Fig 6E,F, Fig S6E). The effects of MCP::BFP co-expression were minor compared to those of MCP::GFP::G3BP (Fig 6E,F).

To determine whether this tethering effect was a stress-specific, we examined the effect in unstressed cells and stressed cells separately. Although all reporters showed effects of tethering in arsenite-treated cells, no substantial differences between tethered and untethered controls were observed in unstressed cells (Fig S6F,G), arguing that tethering to SGs via G3BP reinforces translation in a stress-dependent manner and consistent with a model in which this is due to SG recruitment.

To further distinguish between SG and G3BP function, we examined whether the effect of tethering was specific to G3BPs. To do this, we measured the TEs of reporters tethered to SGs expressing MCP fused to CAPRIN1 (MCP::RFP::CAPRIN1). Although we were able to recover cell

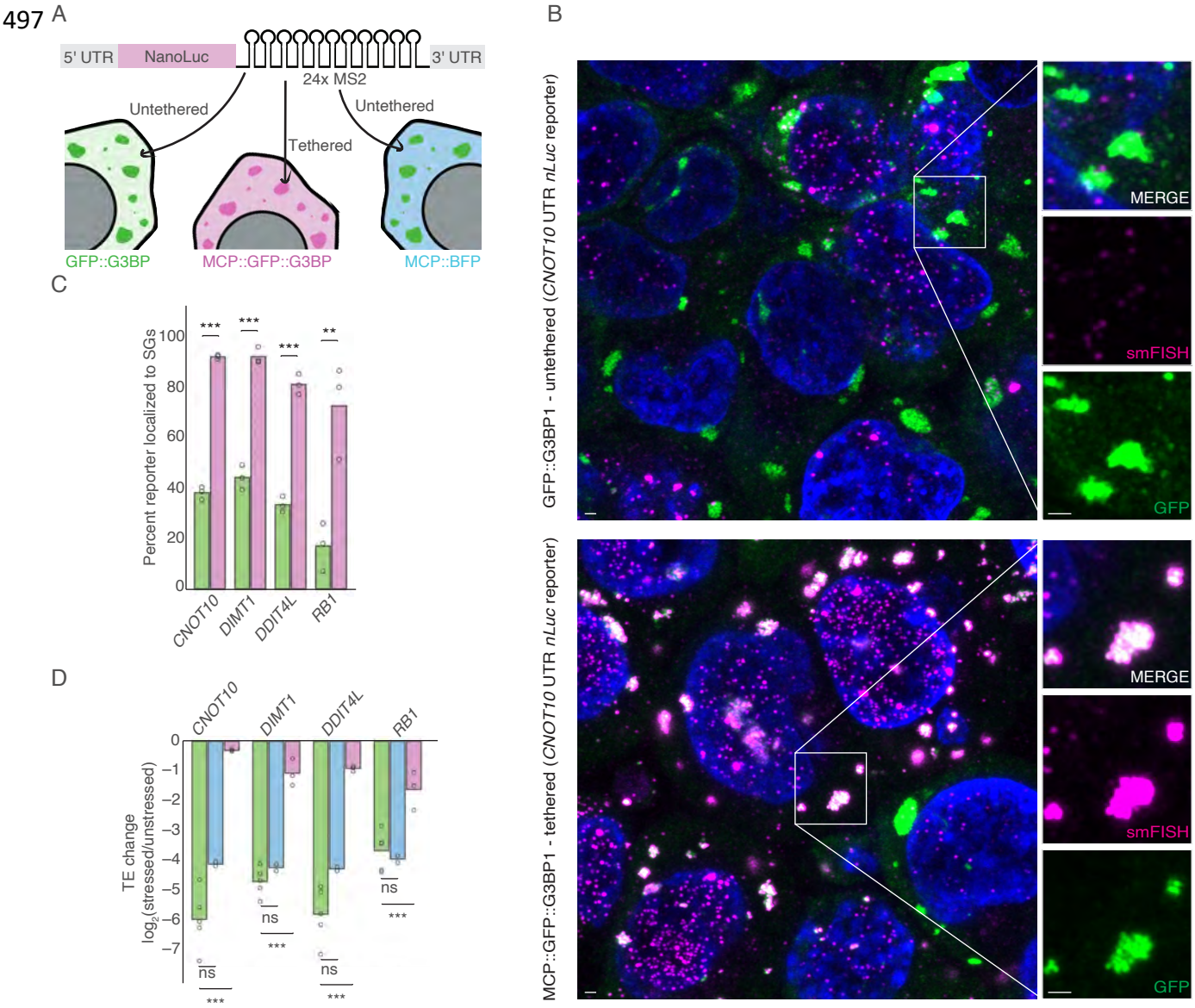

Figure 6. Tethering to SGs via G3BP1 imparts resistance to ISR translation shutdown. (A) Schematic representation of SG tethering experiment. The 5' and 3' UTRs of an mRNA of interest were appended to a nanoluciferase reporter (NanoLuc) that contained 24x repeats of the MS2 hairpin. The reporter was then expressed in each of three different HCT116-derived cell lines: a line expressing endogenous G3BP1 tagged with GFP (GFP::G3BP), a line expressing endogenous G3BP1 tagged with the MS2 coat protein (MCP) fused to GFP (MCP::GFP::G3BP), and a line expressing endogenous G3BP1 tagged with GFP and expressing MCP fused to ectopic BFP (MCP::BFP). **(B)** Tethering a luciferase reporter to SGs via G3BP1. HCT116 cells expressing a NanoLuc reporter bearing 5' and 3' UTRs from *CNOT10* and endogenous G3BP1 tagged with either GFP (top) or MCP::GFP (bottom) were stressed with 500 µM sodium arsenite for 90 min. Images show localization of G3BP in green and smFISH of NanoLuc reporter molecules in magenta (scale bars, 1 µm). White boxes highlight insets that are expanded on the right. **(C)** SG tethering efficiency. Percent of cytoplasmic reporter molecules localized to SGs in untethered cells (green) and to SGs in tethered cells (pink) are shown for reporters with 5' and 3' UTRs of the indicated genes. Points show values for at least three biological replicates (** $p \leq 0.01$, *** $p \leq 0.001$, Welch's two-sample t-test). The average SG tethering efficiency for the four different reporters was 33 for untethered cells and 86 for tethered cells, with standard deviations of 12% and 9%, respectively.

(D) G3BP1-tethered ISR translation response. Plotted for each reporter is the change in TE caused by arsenite stress (500 µM sodium arsenite for 90 min) in untethered cells (green), untethered cells expressing MCP::BFP (blue), or tethered cells (pink) (ns, not significant). The average $\log_2$ FC in TE for the ISR translation response was –5.05 for untethered cells, –4.15 for MCP::BFP expressing cells, and –0.98 for tethered cells; otherwise, as in (C).

using another MCP-tagged SG protein. Accordingly, reporters were integrated into a cell line lines for only three of the four reporters, for all three, recruitment to SGs robust, resembling that observed with G3BP tethering (Fig S6H,I). To measure the effects of this alternative tethering strategy, we expressed both the reporters and doxycycline-inducible, MCP tagged CAPRIN1 in our AID::G3BP cell line. With this combination, we could assess the effects of tethering the reporter to SGs via CAPRIN1 and test whether those affects were dependent on the presence of G3BPs and SGs using the AID degron system.

To induce MCP-tagged CAPRIN1 without depleting the AID-tagged G3BPs, we treated cells with both 1 µg/ml doxycycline and 200 µM auxinole, a small-molecule inhibitor of OsTIR1 activity. Robust expression of MCP-tagged CAPRIN1 was observed, with minimal inhibition of SG formation due to G3BP depletion (Fig S6J – L). Under these conditions, our reporters, tethered to SGs via CAPRIN1, significantly retained translation following arsenite, compared to uninduced, untethered cells, which showed that this effect was not specific to tethering via G3BPs. We note that the effect size observed with CAPRIN1 tethering was smaller than that observed which G3BP tethering, which might be attributable to the smaller translation inhibition observed upon stress, potentially due to differences in cell line background. Furthermore, when cells were instead treated with both 1 µg/ml doxycycline and 500 µM IAA to degrade G3BPs and prevent SG formation, this retention of translation was abolished (Fig S6M), which indicated that this effect of tethering required the presence of G3BPs. Taken together, the results of these tethering experiments indicated that tethering the 3'UTR of an mRNA to either G3BP1 or CAPRIN1 caused increased recruitment to SGs and imparted resistance to the global reduction in translation due to the ISR—consistent with a model in which localization to SGs grants an mRNA prioritized translation during stress.

DISCUSSION

SGs were once thought to be required for the global repression of translation observed during the ISR.[5,15,20,24,25] This idea fell out of favor as many studies showed that cells incapable of forming SGs still mount an ISR translation response.[1,5,26] Since then, additional evidence has led to the hypothesis that SGs, far from being required for the ISR translation response, have no function and are the unavoidable, incidental byproducts of increased RNA availability due to translation repression.[34,35] Here, we propose a model in which SGs are neither required for the substantial changes in translation induced during the ISR nor incidental condensates that have no impact on the stress translation response, but instead measurably amplify and reinforce the ISR translation program, thereby leading to a widespread and statistically significant, albeit relatively modest, impact on global translation.

This widespread reinforcement of the ISR is consistent with several observations of SG biology. SGs recruit a wide array of mRNAs and proteins, constituting a significant redistribution

536 of the cytoplasm during stress.[14,17,18] At the same time, SGs contain only ~10% of the
537 cytoplasmic mRNAs and protein molecules,[18,53] which implies that they would be less likely to
538 have dramatic impacts on cellular outcomes from stress and more likely to play more subtle
539 tuning roles on expression of many different genes.
540 Indeed, a recent study investigating the impact of SGs during viral infection reports that,
541 although SGs are not required for the innate immune response to viral infection or double-
542 stranded RNA (dsRNA), they play a role in tuning that response.[51] However, instead of
543 amplifying the stress response as we saw during arsenite and heat stress, SGs are reported to
544 act as shock absorbers in response to viral infection, limiting the extent of the ISR transcriptional
545 response.[51] The difference in orientation of these potential tuning functions might be explained
546 by the difference in the nature of their stressors and composition of their SGs. Different stresses
547 lead not only to different stress responses but also to distinct stress granules with distinct
548 compositions.[19,39] Thus, viral infection or treatment with dsRNA may result in SGs with very
549 different composition and biology. Indeed, the granules formed in response to dsRNA tend to be
550 smaller than those formed by arsenite or heat shock and tend to only weakly recruit PABPC1
551 and polyadenylated mRNAs, with some of the RNAs most enriched in canonical SGs such as
552 AHNAK and NORAD not present in dsRNA SGs.[65] Furthermore, whereas canonical SGs require
553 the phosphorylation of eIF2α, granules formed in response to dsRNA do not require the dsRNA-
554 dependent eIF2α kinase PKR for their formation.[51,65] Moreover, the response to viral infection
555 might differ between different cells or viruses, in that the shock-absorber function is not
556 reported to apply in other conditions designed to induce viral stress.[66] All of this is further
557 complicated by the presence of RNAse L bodies (RLBs) which also form in response to viral
558 infection and share markers with SGs, such as G3BPs.[67] Thus, although our results seem likely to
559 be generalizable across canonical SGs that require eIF2α phosphorylation, granules formed
560 under viral infection appear to have different effects.
561 In presenting a model of SGs functioning to reinforce the ISR translation program, we
562 propose that, in addition to repressing translation of some mRNAs, SGs also help to rescue
563 translation of others. SGs have previously been hypothesized to play strictly repressive roles in
564 translation for a number of reasons. First, SGs form in conditions of translation repression and
565 are nucleated by the availability of translationally silent mRNAs, implying that the mRNAs
566 localized to them are not translating.[25,68] Second, although SGs are enriched for small ribosomal
567 subunits and eukaryotic initiation factors, they are not enriched for large ribosomal
568 subunits.[20,28] However, neither of these observations preclude SGs from imparting pro-
569 translation effects. First, the mRNAs in SGs are in dynamic exchange with the cytosol and
570 therefore could transit out to the cytosol after their translation was initiated, which would
571 maintain enrichment for translationally silent mRNAs inside the SGs.[29,30,38] Indeed, translation
572 initiation inside the SG might even lead to expulsion of the mRNA, as the presence of even a
573 single ribosome can prevent an mRNA from localizing to an SG.[69] Second, although 40S and 60S
574 ribosomal subunits in SGs are at different stoichiometries than they are in the cytosol, 60S
575 subunits are not depleted from SGs; their availability is equal to that in the cytosol.[20,28] Indeed,
576 a recent study following the translation of *ATF4* reporter molecules during stress reports that
577 translation in the SG is neither impossible nor a rare event.[30] Thus, these prior observations
578 leave open the possibility that SGs could be sites that lead to privileged translation for a subset
579 of mRNAs.

580 Although this model of mRNAs being preferentially initiated or translated while localized to
581 the SG is perhaps the simplest interpretation of our data, it is not the only interpretation.
582 Another possibility is that while transiting through an SG, mRNAs are licensed to be more
583 efficiently translated, and then, having acquired this licensing, they go on to be translated
584 independent of their localization in the SG or cytosol (Fig 7). Elaborating on this possibility,
585 perhaps an mRNA is translated at the same efficiency inside or outside of the SG, but in either
586 case its TE might be proportional to its dwell time inside of the SG and thus proportional to its
587 likelihood of acquiring the license to be more efficiently translated.
588 This license to translate could be acquired through the binding of either translation
589 machinery or a set of pro-translation RNA-binding proteins. For example, loading of a
590 preinitiation complex (PIC) assembled from the 40S ribosome subunit and initiation factors,
591 which are known to be enriched in SGs,[20,28] could poise a transcript to be more quickly initiated
592 whether in the SG or in the cytosol.[5,14] Similarly, UBAP2L, which enhances the translation of its
593 associated mRNAs, is highly enriched in SGs.[50,70] Perhaps preferential binding of UBAP2L to an
594 SG mRNA could lead to more efficient translation even after the mRNA has diffused out of the
595 SG. Additional interesting candidates for translational licensing are the G3BPs themselves. The
596 G3BPs have been observed to regulate translation and translation machinery.[1,21-23,71,72] G3BPs
597 also exhibit exceptionally high partitioning into SGs, with almost half of G3BP1 localized to SGs
598 in our cell lines.[63] If G3BPs act to license privileged translation, their strong partitioning to SGs
599 might lead to preferential translation of SG-resident transcripts (Fig 7).
600 This proposed increased mRNA licensing in SGs is consistent with the idea that SGs are
601 formed by non-translating RNAs and with the observation that, although an *ATF4* reporter is
602 translated in the SG, it is translated no more efficiently in the SG than in the cytosol.[30] Indeed,
603 we found that *ATF4* mRNA was neither enriched in SGs nor influenced by the presence of SGs,
604 which indicated that other transcripts might better represent mRNAs influenced by SGs.
605 Lastly, it is important to acknowledge the difficulty of distinguishing the function of SGs from
606 the function of the SG-nucleating G3BPs. One approach for inferring the function of SGs is to
607 consider phenotypes consistently observed after different proteins reported to be required for
608 SG formation are depleted. However, many of these proteins, such as the G3BPs, CAPRIN1, and
609 UBAP2L, are thought to form complexes with each other even outside of the context of SGs,
610 meaning that any phenotypes shared between these interacting proteins could be due to the
611 function of complexes that exist independent of SGs.[19,34,35] Moreover, we and others found that
612 the ability to prevent SG formation through depletion of non-G3BP nucleators appears to be
613 stress or cell-type specific, which limits what can be learned regarding general SG function by
614 depleting these factors.
615 Although we have not conclusively distinguished between G3BP function and SG function,
616 five lines of reasoning support the proposal that the ISR translation program is reinforced by SGs
617 rather than by only G3BPs. First, in both our ribosome profiling experiments and our tethered
618 reporter experiments, we found that G3BPs regulate these mRNAs only in the context of stress.
619 Second, although our SG purifications did rely on the IP of G3BPs, this IP was performed
620 specifically on the cellular fraction that pellets after centrifugation at 18,000*g*, which removes
621 most cytosolic G3BP.[17,18,52,73] Thus, our SG transcriptomes should be substantially enriched for
622 the content of G3BP-positive SGs and not simply the G3BP-RNA interactome. Furthermore, we
623 were able to identify similar trends in data from SG-enriched fractions that do not require IP of

G3BPs.[53] Third, we found that formation of OptoGranules, which manipulates only localization of G3BPs, was sufficient to trigger a translation response, and that the content of the OptoGranule was what determined which mRNAs were regulated. Fourth, we found that tethering reporter mRNAs to SGs was sufficient to impart resistance to stress induced translation shut down, whether tethered by G3BP1 or CAPRIN1. Although G3BPs and CAPRIN1 are thought to be binding partners[1], this result indicates that this effect does not require direct recruitment via G3BPs. Fifth, in distinguishing between SG- and G3BP-centric models, we should not dismiss the possibility that both G3BPs and SGs contribute to this translation reinforcement. If G3BPs are a licensing factor for improved translation during stress, and are also strongly partitioned to SGs, perhaps the effects we observe are direct effects of G3BP binding to mRNA, and that recruitment to SGs is a molecular strategy to increase interaction with G3BPs during stress, therefor reinforcing translation of a subset of privileged mRNAs. Although these considerations do not conclusively distinguish between SG and G3BP function, they do support the proposal that SGs are a functional condensate responsible for reinforcing the ISR translation program.

644

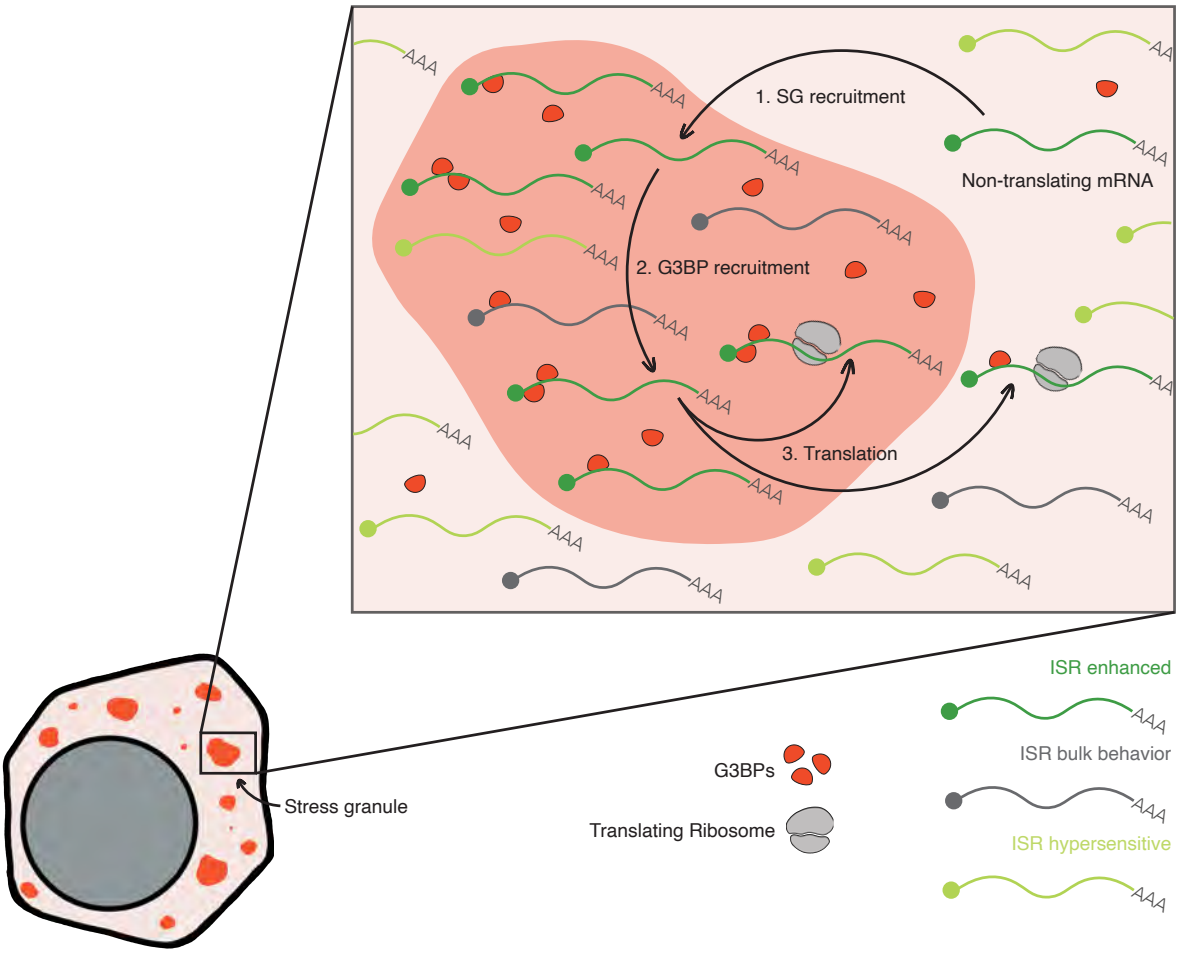

Figure 7. A Plausible Model of SG Translation Control. This model reconciles the previous observation that mRNAs devoid of ribosomes are preferentially recruited to SGs with our observation that mRNAs that are translationally enhanced during the ISR are enriched in SGs, further enhancing their translation. In this model, 1) ISR-enhanced transcripts are preferentially recruited to SGs between cycles of translation, when they lack ribosomes. This preferential recruitment might be the result of various factors, including transcript length, presence of relevant RBP-binding motifs, or translation state prior to stress. 2) As a consequence of being recruited to SGs, these transcripts are licensed for translation. One possible mechanism of licensing (depicted here) is the recruitment of G3BPs, which are highly enriched in SGs. 3) After this licensing, this model is agnostic to the location of the translation that follows. The transcript might diffuse out to the cytosol, or could remain inside the SG. Once these transcripts complete their translation, they would be available to, once again, be preferentially recruited to (or retained in) the granule.

645
646
647
648
649
650
651

652 ## Methods

653 **Cell culture**

654 All cells were cultured at 37°C with 5% CO_2 using McCoy's 5A medium supplemented with 10%
655 fetal bovine serum (FBS) and 2mM L-glutamine. HCT116 (CCL-247 from ATCC) were obtained
656 from the Young lab.
657

658 **Cell-line construction**

659 **Cas9 mediated editing.** Fusion proteins were introduced into the endogenous locus of genes
660 using the Cas9 genome editing system. The 5' and 3' homology arms (each 200 – 700 bp)
661 flanking an insertion site were either amplified from genomic DNA of the parental cell line or
662 from gblock gene fragments (IDT) cloned into a rescue template plasmid, flanking the fusion
663 protein sequence. This plasmid, along with pX330 plasmid expressing a Cas9 guide RNA, was
664 reverse transfected into the parental cell line using lipofectamine 3000 transfection reagent in a
665 6-well dish at 100% confluency. After 48 h, these cells of each well were expanded to a 10 cm
666 dish and cultured for an additional 24 h. Cells with strong signal from the fusion protein
667 fluorescence were single-cell sorted into 96-well plates using flow cytometry. Colonies derived
668 from single cells were grown, expanded, and screened by PCR genotyping and western blotting.
669 Unless otherwise stated, all endogenously edited cell lines were edited homozygously.
670 **PiggyBac editing.** Exogenous genes were introduced into cells using the PiggyBac transposon
671 system. The exogenous gene was either amplified from genomic DNA of the parental cell line or
672 from gblock gene fragments (IDT) and cloned into a plasmid expressing the PiggyBac inverted-
673 repeat sequences along with a selection marker for either hygromycin, puromycin, or
674 blasticidin. This plasmid, along with the super PiggyBac transposase expression vector (System
675 Biosciences #PB210PA-1), was reverse transfected into the parental cell line using lipofectamine
676 3000 transfection reagent (Thermo #L3000015) in a 6-well dish at 100% confluency. After 48 h,
677 cells of each well were expanded to a 10 cm dish and successfully edited cells were selected for
678 using the appropriate antibiotic. For cases in which a fluorescent protein had been transposed
679 into the genome, cells expressing the protein at the appropriate level were single-cell sorted
680 into 96-well plates by flow cytometry. Colonies derived from single cells were grown, expanded,
681 and screened by either microscopy, western blotting, or both.
682

683 **Ribo-spike production**

684 **In vitro transcription.** Ribo-spike mRNA was generated using mMessage mMachine kit (Thermo
685 # AM1344) following the standard T7 protocol. DNA transcription template was generated by
686 PCR of a plasmid template encoding the firefly luciferase coding region (*fLuc*) preceded by the
687 T7 promotor and followed by an encoded poly(A) tail of 30 nt length. The resulting PCR product
688 was purified using phenol–chloroform extraction followed by ethanol precipitation and was size
689 selected and purified from an agarose gel using the "freeze and squeeze" method in which the
690 gel slice was frozen at –80°C for 30 min, followed by centrifugation at 21,000*g* for 5 min.[74] The
691 eluted DNA was then concentrated by an additional ethanol precipitation and added to the
692 mMessage mMachine in vitro transcription reaction, incubated for at 37°C for 2 h, and then
693 treated with TURBO DNAse for 15 min at 37°C. RNA from the in vitro transcription reaction was
694 recovered by passing the reaction over a tris-buffered micro bio-spin p30 gel column (Bio-Rad

695 #7326223) centrifuging at 1000*g* for 4 min. The resulting flowthrough was then purified by
696 phenol–chloroform extraction and ethanol precipitation, and then resuspended in water. RNA
697 was examined by running an aliquot on a 4% urea–polyacrylamide denaturing gel and staining
698 with Sybr Gold (Thermo #S11494).
699 **In vitro translation.** The *fLuc* mRNA was in vitro translated using a rabbit reticulocyte lysate
700 system (Promega #L4151) following the standard non-nuclease treated protocol, with the
701 exception of using a shorter incubation time to maximize ribosome occupancy. The reaction was
702 assembled by combining 0.06 µM *fLuc* mRNA with reticulocyte lysate, 0.02 mM complete amino
703 acid mixture, 0.8 units/µl RNAsein ribonuclease inhibitor, 0.01 M creatine phosphate, 0.05
704 mg/ml creatine phosphokinase, 2 mM DTT, 0.05 mg/ml tRNA, 80 mM potassium acetate, and
705 0.5 mM magnesium acetate in 23 117 µl reactions. The reactions were incubated at 30°C for 15
706 min, cooled on ice and treated with 0.1 mg/ml cycloheximide to block ribosome translocation.
707 Reactions were then combined, mixed, aliquoted, snap frozen in liquid nitrogen, and stored at –
708 80°C.
709
710 **IAA-induced protein depletion**
711 HCT116 cells were engineered using the PiggyBac system to express multiple copies of
712 doxycycline-inducible *OsTIR1*. These cells were then also engineered using Cas9 to expressed
713 AID-tagged fusion proteins edited at their endogenous loci. Cells expressing fusion proteins
714 were first doxycycline-induced for 4 h and were then treated with 500 µM IAA (Gold Bio #I-110-
715 25) to induce rapid (< 3 h) depletion of the AID-fusion protein. Depletion was confirmed by
716 microscopy, western blot, or both. When confirming by western, as was the case with G3BP1,
717 G3BP2, and CAPRIN1 proteins, antibodies raised directly against the target proteins were used
718 to enable detection of untagged alleles, if present. Where indicated, non-depleted controls
719 were treated with 200 µM auxinole (Aobious #AOB8812) to minimize background protein
720 degradation.[75] Unless otherwise stated, all other non-depleted control cells were treated only
721 with ethanol, the solvent used for IAA. Previous work has shown that addition of IAA alone does
722 not affect translation.[76]
723
724 **Stress conditions**
725 For oxidative stress, unless otherwise stated, cells were treated with media containing 500 µM
726 sodium arsenite (Sigma #93289) for 1 h. For heat shock, media was separately heated to 45°C.
727 Media was removed from cells previously grown in a 37°C, rapidly replaced with 45°C media,
728 and then cells were quickly placed in a 45°C incubator for 25 min.
729
730 **Doxycycline induction**
731 For all doxycycline inductions, cells were treated with 1 µg/ml doxycycline (Clonetech Takara Bio
732 #631311) for indicated amount of time.
733
734 **Tethered reporter TE experiments**
735 To measure changes in TE for the nanoluciferase reporters (NanoLuc), cells expressing a reporter
736 containing selected 5' and 3' UTRs, NanoLuc fused to an ecDHFR domain and 24x MS2 stem
737 loops, were harvested using trypsin, centrifuged at 300*g* for 5 min, aspirated, washed with cold
738 PBS, lysed in buffer containing 10 mM Tris HCl pH 7.5, 5 mM $MgCl_2$, 100 mM KCl, 1% triton, 1x

739 cOmplete mini tablet (EDTA free), and 0.02 U/µl SUPERase-In RNase inhibitor, and depleted of
740 nuclei by centrifuging at 1300*g* for 10 min at 4°C. Nuclear-depleted supernatant was then
741 transferred to a new tube and flash frozen using liquid nitrogen and stored at –80°C. Cells were
742 then assayed for total protein using bicinchoninic acid, luciferase production, and reporter
743 mRNA using RT-quantitative PCR (RT-qPCR) comparing to the *GAPDH* mRNA, which did not
744 change in abundance during treatment with sodium arsenite (Fig S6C). Change in translation
745 efficiency was then calculated as
746

747 $$\Delta \mathrm{TE}_{\mathrm{MCP/GFP}} = \frac{\Delta \mathrm{NanoLuc\ signal}_{\mathrm{MCP/GFP}}}{\Delta \mathrm{mRNA}_{\mathrm{MCP/GFP}}} = \frac{\dfrac{\mathrm{NanoLuc\ signal/Total\ Protein}_{\mathrm{MCP}}}{\mathrm{NanoLuc\ signal/Total\ Protein}_{\mathrm{GFP}}}}{\dfrac{\textit{NanoLuc}\ \mathrm{mRNA}/\textit{GAPDH}\ \mathrm{mRNA}_{\mathrm{MCP}}}{\textit{NanoLuc}\ \mathrm{mRNA}/\textit{GAPDH}\ \mathrm{mRNA}_{\mathrm{GFP}}}}$$

748
749 where MCP indicates the reporter being expressed in a cell line expressing MCP::BFP or
750 MCP::GFP::G3BP1, and GFP indicates the reporter being expressed in a cell line expressing
751 GFP::G3BP1.
752 **Luciferase Assays.** Luciferase assays were conducted using the standard protocol of the
753 Luciferase Reporter Assay System (Promega #E1910). Cell lysates were analyzed in 48-well
754 microplate format at room temperature using a GloMax microplate reader and luminometer
755 device (Promega #GM3000).
756 **RT-qPCR.** RNA was extracted using TRI reagent (sigma #93289), precipitated using ethanol and
757 linear acrylamide (thermo #J67830-XF) and resuspended in water. RT reactions were performed
758 using a Quantitect RT kit following kit protocols. Genomic DNA was first eliminated using 7x
759 gDNA wipeout buffer and incubating at 42°C for 2–5 min. Reactions were then placed on ice, RT
760 reagents were added, and then RT was performed at 42°C for 30 min. RT enzyme was heat
761 inactivated by incubating at 95°C for 3 min. cDNA product was then diluted 1:2 in water and
762 stored at –20°C. qPCR was then performed using the PowerUP SYBR Green qPCR master mix
763 and primers targeting either the *NanoLuc* or *GAPDH* sequences. Each sample was run in
764 technical triplicate PCR using a QuantStudio 6 Pro RT-PCR System (Thermo).
765
766 **Blue-light LED treatment**
767 Cells were exposed to blue light for indicated amounts of time using a 12 inch square LED Grow
768 Light System with 225 x 14W Blue LEDs (HQRP #884667106091218) mounted inside of their cell
769 culture incubator.
770
771 **Fluorescence recovery after photobleaching**
772 Cells were bleached using a blue light (488 nm) laser, followed by green channel imaging every
773 second for 3 min. Imaging was performed using an Andor Revolution Spinning Disk Confocal
774 with FRAPPA system. FRAP Analysis was performed using Fiji (ImageJ).
775
776 **Immunofluoresence and live imaging**
777 Cells were grown in plastic Nunc Cell Culture Treated Multidishes (Thermo #140675). For live
778 imaging, cells were aspirated of their cell growth media and replaced with PBS. For
779 immunofluorescence, cells were fixed using 3.7% formaldehyde in PBS at room temperature for

780 15 min, washed with PBS for 5 min three times, blocked using normal goat serum diluted in PBS
781 with 0.3% triton for at least 1 h, then treated with primary antibody diluted in 1% normal goat
782 serum, 0.3% triton, and PBS. Primary antibody treatments were performed overnight at 4°C.
783 Cells were then washed in PBS for 5 min three times and treated with secondary antibody using
784 same dilution buffer for 1–2 h at room temperature. Cells were washed a final time with PBS
785 and mounted using mounting media containing DAPI (VECTASHIELD #H-2000-10). Imaging was
786 performed on a Nikon Ti automated inverted microscope with incubation enclosure. Images
787 were analyzed using Fiji (Image J).
788
789 **smFISH**
790 For smFISH, cells were plated in glass bottom, 10 mm, 24 well plates (MatTek Corporation
791 #P24G-1.5-10-F). Cells were prepared following the standard Stellaris RNA FISH protocol for
792 adherent cells (Biosearch Technologies). Cells were fixed using 3.7% formaldehyde in PBS at
793 room temperature for 10 min. Cells were then permeabilized using 70% ethanol for at least 1 h
794 at 4°C. Cells were washed with Wash buffer A and incubated at room temperature for 5 min.
795 Wash buffer A was aspirated and cells were treated with approximately 30 µl of 125 nM FISH
796 probe diluted in hybridization buffer. The plate was sealed with parafilm and stored in dark
797 humid chamber overnight at 37°C. Cells were then washed with wash buffer A for 30 min at
798 37°C , then washed with wash buffer B for 5 min and mounted with mounting media containing
799 DAPI (VECTASHIELD #H-2000-10). smFISH imaging was performed using a Zeiss LSM 980 with
800 Airyscan 2 Laser Scanning Confocal imaging system with Zeiss AxioObserver motorized inverted
801 microscope stand, DIC optics, and a motorized XYZ stage. Images were analyzed using IMARIS.
802
803 **Western Blots**
804 Samples used for western blots were lysed by boiling in NuPAGE LDS Sample Buffer (Thermo #
805 NP0007) diluted to 1x concentration and supplemented with 1 mM DTT. Samples were run on
806 NuPAGE 4 to 12% Bis-Tris 1.0 mm miniprotein gels (Thermo #NP0321BOX), then transferred to
807 0.2µM PVDF transfer membranes (Thermo #22860). All protein gels and transfers were run
808 using a mini gel tank (Thermo #A25977) with protein gels run at 200V for 80 min and transfers
809 run at 30V for 60 min. Transferred membranes were blocked in PBS with 1% Triton and 5% milk
810 for at least 1 h at room temperature before they were transferred to primary antibody diluted in
811 the same buffer at 4°C. Primary antibody was applied overnight followed by at least three 5 min
812 washes with the same blocking buffer, secondary antibody diluted in the same buffer for 30 min
813 at room temperature, and three 5 min washes in the same buffer. Westerns were imaged using
814 the Odyssey CLx imaging system by LI-COR. All western blot quantifications were done using
815 Fiji/ImageJ software.
816
817 **Ribosome profiling and matched RNA-seq**
818 HCT116 cells were cultured in a 15 cm dish, washed twice with cold PBS, scraped into lysis
819 buffer containing 10 mM Tris HCl pH 7.5, 5 mM $MgCl_2$, 100 mM KCl, 1% triton, 2 mM DTT, 1x
820 cOmplete mini tablet (EDTA free), 0.3 U/µl RNasin Plus RNase inhibitor, and 1:60 dilution of
821 ribo-spike. Cells were lysed by passing through 26G ½ inch needle at least 7 times. Lysates were
822 depleted of nuclei by centrifugation at 1300*g* for 10 min at 4°C, divided into aliquots for ribo-

seq and matched RNA libraries, and snap frozen using liquid nitrogen. Ribosome profiling and matched RNA seq libraries were then prepared according to previously established protocol,[77] a detailed version of which is available at http://bartellab.wi.mit.edu/ protocols.html. Sequencing was performed on an Illumina HiSeq 2500 using 50 cycles. Only reads mapping to ORFs of GRCh38-annotated genes, fluorescent protein-coding genes, the OsTIR1 gene, or the *fLuc* gene were used. Reads mapping to the first 50 nt of each ORF were excluded. Reads mapping to heme-related genes from the rabbit genome (Broad/oryCun2) were also excluded. TE changes were calculated and count depth normalization was performed for using DESeq2.[78]

Isolation of RNA from HCT116 cells and SG cores for RNA sequencing

Isolation and sequencing of SG cores was adapted from an established protocol.[18,52] HCT116 cells were cultured in a 24.5 cm square dish, washed with PBS, scraped into PBS, centrifuged at 1500*g* for 3 min, aspirated to remove liquid, and snap frozen in liquid nitrogen. Frozen cell pellets were thawed in lysis buffer (50 mM Tris HCl pH 7.4, 2 mM MgOAc, 10 mM $MgCl_2$, 100 mM KOAc, 0.1% NP40, 0.5 mM DTT, 1x cOmplete mini tablet (EDTA free), and 1 U/µl RNasin Plus RNase inhibitor). Cells were lysed by passing through 26G ½ inch needle at least seven times. Lysates were depleted of their nuclei by centrifugation at 1000*g* for 5 min at 4°C. 5% of this nuclear-depleted sample was aliquoted and snap frozen in liquid nitrogen and stored at –80°C as the cytoplasmic fraction. The remaining 95% was used to isolate the SG fraction. Sample was centrifuged at 18,000*g* for 20 min at 4°C. Pellet was resuspended in 1 ml lysis buffer and allowed to turn end-over-end for at least 10 min at 4°C. Once resuspended, sample was centrifuged again at 18,000*g* for 20 min at 4°C. The pellet was resuspended in 300 µl lysis buffer and centrifuged at 850*g* for 2 min at 4°C. The supernatant was taken and incubated with 6 µg of G3BP2 antibody (Bethyl Laboratories #A302-040A) overnight at 4°C, rotating end-over-end. Sample was centrifuged at 18,000*g* for 20 min at 4°C to remove unbound antibody, and the pellet was resuspended in 500 µl lysis buffer. 625 µl of M-280 sheep, anti-rabbit IgG dynabeads (Thermo # 11204D) were then added to the sample and incubated for at least 3 h at 4°C, rotating end-over-end. Beads were washed with buffer containing 20 mM Tris HCl pH 8.0 and 50 mM NaCl and eluted using a high-salt buffer (10mM Tris HCl pH 7.5, 1M NaCl, 5% 1,6 hexanediol, 5mM $MgCl_2$, 100mM KCl, 1% triton, 2mM DTT, 1x cOmplete mini tablet (EDTA free), and 0.3 U/µl RNasin Plus RNase inhibitor), turning end-over-end for at least 4 h. Eluate was snap frozen using liquid nitrogen and stored at –80°C as the SG fraction. RNA-sequencing libraries were then prepared from the cytoplasmic and SG fractions in parallel, following the protocol used for the RNA-sequencing libraries that matched the ribosome profiling. SG enrichment values were calculated using DESeq2.[78]

Statistical analysis and comparison with published datasets

Plots and statistical analyses were performed using R. Statistical tests and parameters are shown in figure legends. Additional data were obtained from publicly available datasets associated with published work[18,43,46,53,54] and re-analyzed using R.

Figure S1

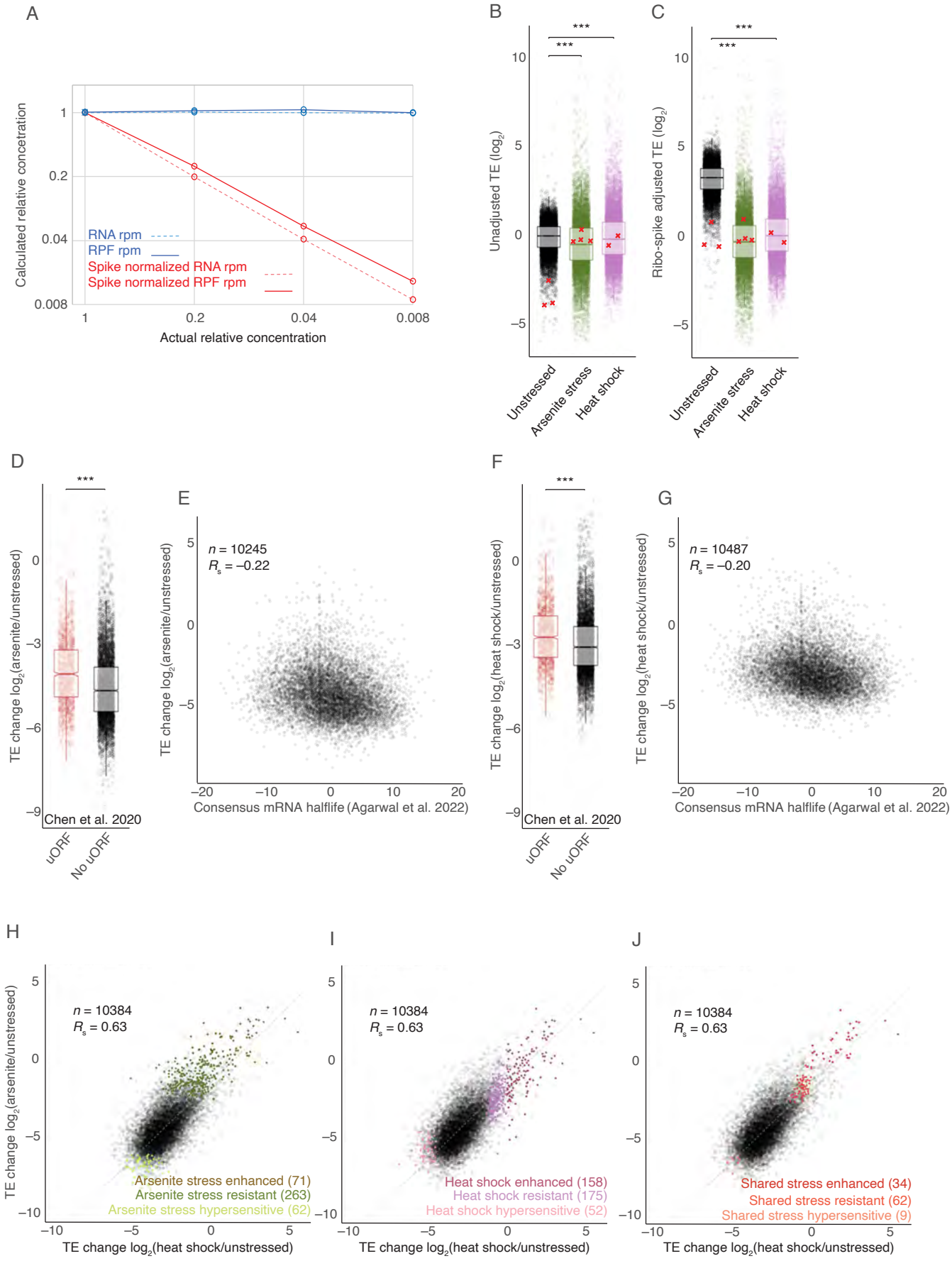
A
Calculated relative concetration
Actual relative concentration
RNA rpm
RPF rpm
Spike normalized RNA rpm
Spike normalized RPF rpm
B
Unadjusted TE (log2)
Unstressed
Arsenite stress
Heat shock
C
Ribo-spike adjusted TE (log2)
D
TE change log2(arsenite/unstressed)
Chen et al. 2020
uORF
No uORF
E
n = 10245
Rs = –0.22
Consensus mRNA halflife (Agarwal et al. 2022)
F
TE change log2(heat shock/unstressed)
G
n = 10487
Rs = –0.20
H
n = 10384
Rs = 0.63
Arsenite stress enhanced (71)
Arsenite stress resistant (263)
Arsenite stress hypersensitive (62)
TE change log2(heat shock/unstressed)
I
Heat shock enhanced (158)
Heat shock resistant (175)
Heat shock hypersensitive (52)
J
Shared stress enhanced (34)
Shared stress resistant (62)
Shared stress hypersensitive (9)

Figure S1. Heat shock and oxidative stress illicit similar but distinct ISR translation programs. **(A)** Quantification of ribo-spike. Cytoplasmic extract from HCT116 cells was serially diluted to achieve the indicated relative concentrations, and then a constant amount of ribo-spike was added to each sample before ribosome profiling and RNA-seq analyses. Plotted are the relative concentrations of total mRNA (dashed line) and RPFs (solid line) as calculated from the 1000 most highly expressed genes, using no-spike controls (blue) and ribo-spike normalized samples (red) as a function of the actual relative concentrations. **(B)** Relative TE measurements before adjusting for ribo-spike. Plotted with circles are the average $\log_2$ TE values (line, median; notch, 95% confidence interval; box, quartiles; whiskers, 1.5 x IQR) calculated for mRNAs from either untreated cells (black, three replicates), cells treated with 500 µM sodium arsenite for 1 h (green, four replicates), or cells treated with heat shock at 45°C for 25 min (pink, 2 replicates). Red Xs denote the ribo-spike TE values (one for each replicate). Statistical significance was calculated based on ribo-spike values alone (***, $p \leq 0.001$; Welch's two-sample t-test). **(C)** TE measurements of panel B after adjusting for ribo-spike; otherwise, as in (B). Note that statistical significance is determined in panel B, using ribo-spike values prior to adjustment (***, $p \leq 0.001$). **(D)** Preferential translation of mRNAs containing uORFs during arsenite stress. The plots indicate $\log_2$ FC in TE caused by arsenite for mRNAs containing at least one uORF and those containing no uORFs, according to annotations from Chen et al. (2020)[43] (line, median; notch, 95% confidence interval; box, quartiles; whiskers, 1.5 x IQR); ***, $p \leq 0.001$; Welch's two-sample t-test). **(E)** Relationship between translation during arsenite stress and mRNA half-lives. The plots indicate the $\log_2$ FC in TE due to arsenite as a function of the mean-normalized half-life (PC1) of mRNAs as calculated from consensus of multiple human cell data sets by Agarwal et al. (2022).[46] *n* indicates number of unique mRNAs. **(F)** Preferential translation of mRNAs containing uORFs during heat shock. Plots indicate $\log_2$ FC in TE caused by treatment with 45°C heat shock; otherwise, as in (D). **(G)** Relationship between translation during heat shock and mRNA half-lives. The plots indicate the $\log_2$ FC in TE due to heat shock as a function of the mean-normalized half-life of mRNAs; otherwise, as in (E). **(H – J)** Comparison of arsenite stress and heat shock ISR translation programs. Plotted for each mRNA are changes in TE caused by arsenite as a function of changes in TE caused by heat shock. Points for mRNAs classified as either stress-enhanced, stress-resistant, or stress-hypersensitive mRNAs in either arsenite stress (D), heat shock (E), or both (F) are colored. *n* indicates number of genes; R_s indicates Spearman coefficient.

Figure S2

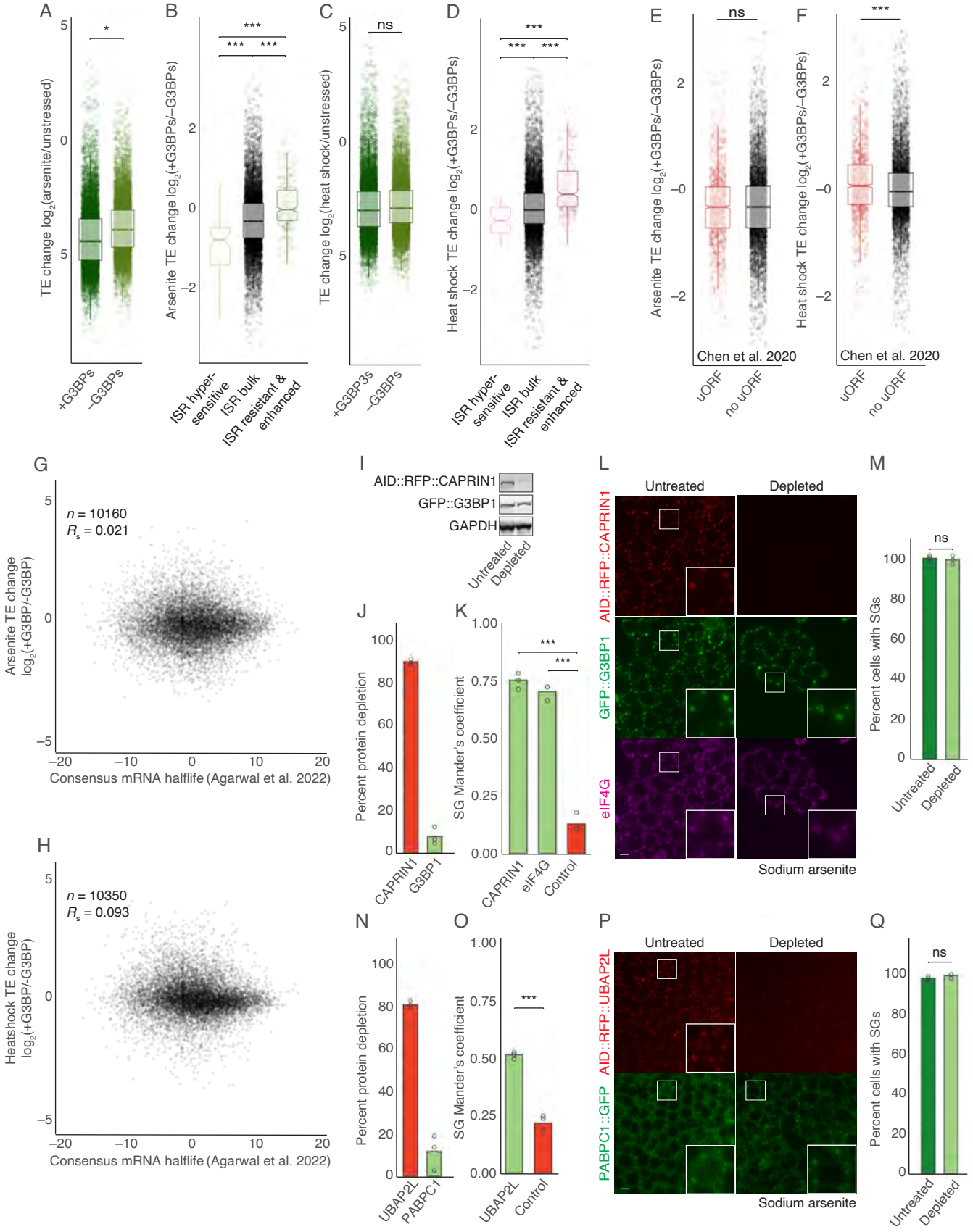
A
B
C
D
E
F
TE change log2(arsenite/unstressed)
Arsenite TE change log2(+G3BPs/−G3BPs)
TE change log2(heat shock/unstressed)
Heat shock TE change log2(+G3BPs/−G3BPs)
Arsenite TE change log2(+G3BPs/−G3BPs)
Heat shock TE change log2(+G3BPs/−G3BPs)
+G3BPs
−G3BPs
+G3BP3s
−G3BPs
ISR hyper-sensitive
ISR bulk
ISR resistant & enhanced
uORF
no uORF
Chen et al. 2020
ns
G
H
n = 10160
Rs = 0.021
n = 10350
Rs = 0.093
Arsenite TE change log2(+G3BP/-G3BP)
Heatshock TE change log2(+G3BP/-G3BP)
Consensus mRNA halflife (Agarwal et al. 2022)
I
AID::RFP::CAPRIN1
GFP::G3BP1
GAPDH
Untreated
Depleted
J
K
N
O
Percent protein depletion
SG Mander's coefficient
CAPRIN1
G3BP1
eIF4G
Control
UBAP2L
PABPC1
L
M
P
Q
Untreated
Depleted
AID::RFP::CAPRIN1
GFP::G3BP1
eIF4G
AID::RFP::UBAP2L
PABPC1::GFP
Sodium arsenite
Percent cells with SGs

Figure S2. Neither CAPRIN1 nor UBAP2L are required for SG formation in HCT116 cells. (A) The ISR translation response to arsenite stress, either with or without G3BPs. The plots indicate the $\log_2$ FC in TE caused by arsenite stress in either untreated HCT116 cells or cells depleted of their G3BPs by addition of 500 µM IAA (line, median; notch, 95% confidence interval; box, quartiles; whiskers, 1.5 x IQR). Significance was determined using ribo-spike values, as in Figure S1B (* $p \leq 0.05$, ***, $p \leq 0.001$; Welch's two-sample t-test). **(B)** Comparison of G3BP-dependent translation and ISR translation in HCT116 cells treated with arsenite stress. The plots indicate the $\log_2$ FC in TE due to presence of G3BPs in stressed cells in each of three ISR translation categories: stress-enhanced/resistant, bulk behavior, and stress-hypersensitive (line, median; notch, 95% confidence interval; box, quartiles; whiskers, 1.5 x IQR; ***, $p \leq 0.001$; Welch's two-sample t-test). **(C)** The ISR translation response to heat shock, either with or without G3BPs. ns, not significant; otherwise, as in (A). **(D)** Comparison of G3BP-dependent translation and ISR translation in HCT116 cells treated with heat-shock stress; otherwise, as in (B). **(E)** G3BP-dependent translation of mRNAs containing uORFs during arsenite stress. The plots indicate the $\log_2$ FC in TE due to presence of G3BPs in arsenite-stressed cells for mRNAs containing at least one uORF and those containing no uORFs, according to annotations from Chen et al. (2020)[43] (line, median; notch, 95% confidence interval; box, quartiles; whiskers, 1.5 x IQR); ***, $p \leq 0.001$; Welch's two-sample t-test). **(F)** G3BP-dependent translation of mRNAs containing uORFs during heat stress. The plots indicate the $\log_2$ FC in TE due to presence of G3BPs in heat-stressed cells for mRNAs containing at least one uORF and those containing no uORFs; otherwise as in (E). **(G)** Relationship between G3BP-dependent translation during arsenite stress and mRNA half-lives. The plots indicate the $\log_2$ FC in TE due to presence of G3BPs in arsenite-stressed cells as a function of the mean-normalized half-life (PC1) of mRNAs as calculated from consensus of multiple human cell data sets by Agarwal et al. (2022).[46] *n* indicates number of unique mRNAs. **(H)** Relationship between G3BP-dependent translation during heat stress and mRNA half-lives. The plots indicate the $\log_2$ FC in TE due to presence of G3BPs in heat-stressed cells as a function of the mean-normalized half-life of mRNAs; otherwise, as in (G). **(I)** Depletion of endogenous CAPRIN1 fused to AID. Immunoblots probed for the indicated proteins show specific depletion of AID fusion protein after treatment with 500 µM IAA for 3 h. **(J)** Quantification of protein depletion in (I), normalizing to levels of GAPDH. Points show values for three biological replicates. **(K)** Colocalization of CAPRIN1 in SGs. Quantification of colocalization was performed using Mander's coefficient between G3BP1 and indicated SG marker, comparing to a control image from an irrelevant field of cells (***, $p \leq 0.001$; Welch's two-sample t-test)**. (L)** SG formation despite CAPRIN1 depletion. HCT116 cells were either treated with 500 µM IAA to deplete CAPRIN1 (right) or not treated (left) prior to arsenite stress (500 µM sodium arsenite for 1 h). Images show either CAPRIN1 in red, SG marker protein G3BP1 in green, or SG marker protein eIF4G in magenta (scale bars, 10 µm). **(M)** Quantification of SG formation in (L). Points show values for three biological replicates (ns, not significant). **(N)** Depletion of endogenous UBAP2L fused to AID. Quantification was based on AID::RFP::UBAP2L and PABPC1::GFP fluorescence in homozygously tagged HCT116 cells (images not shown). Points show values for three biological replicates. **(O)** Colocalization of UBAP2L in SGs. Quantification of colocalization was performed using Mander's coefficient between PABPC1 and UBAP2L, comparing to a control image from an irrelevant field of cells (***, $p \leq 0.001$; Welch's two-sample t-test)**. (P)** SG formation despite UBAP2L depletion. HCT116 cells were either treated with 500 µM IAA to

947 deplete UBAP2L (right) or not treated (left) prior to arsenite stress (500 µM sodium arsenite for
948 1 h). Images show either UBAP2L in red or SG marker protein PABPC1 in green; otherwise, as in
949 (L). **(Q)** Quantification of SG formation in (P); otherwise, as in (M).
950
951
952
953
954
955
956
957
958
959
960
961
962
963
964
965
966
967
968
969
970
971
972
973
974
975
976
977
978
979
980
981
982
983
984
985
986
987
988
989

Figure S3

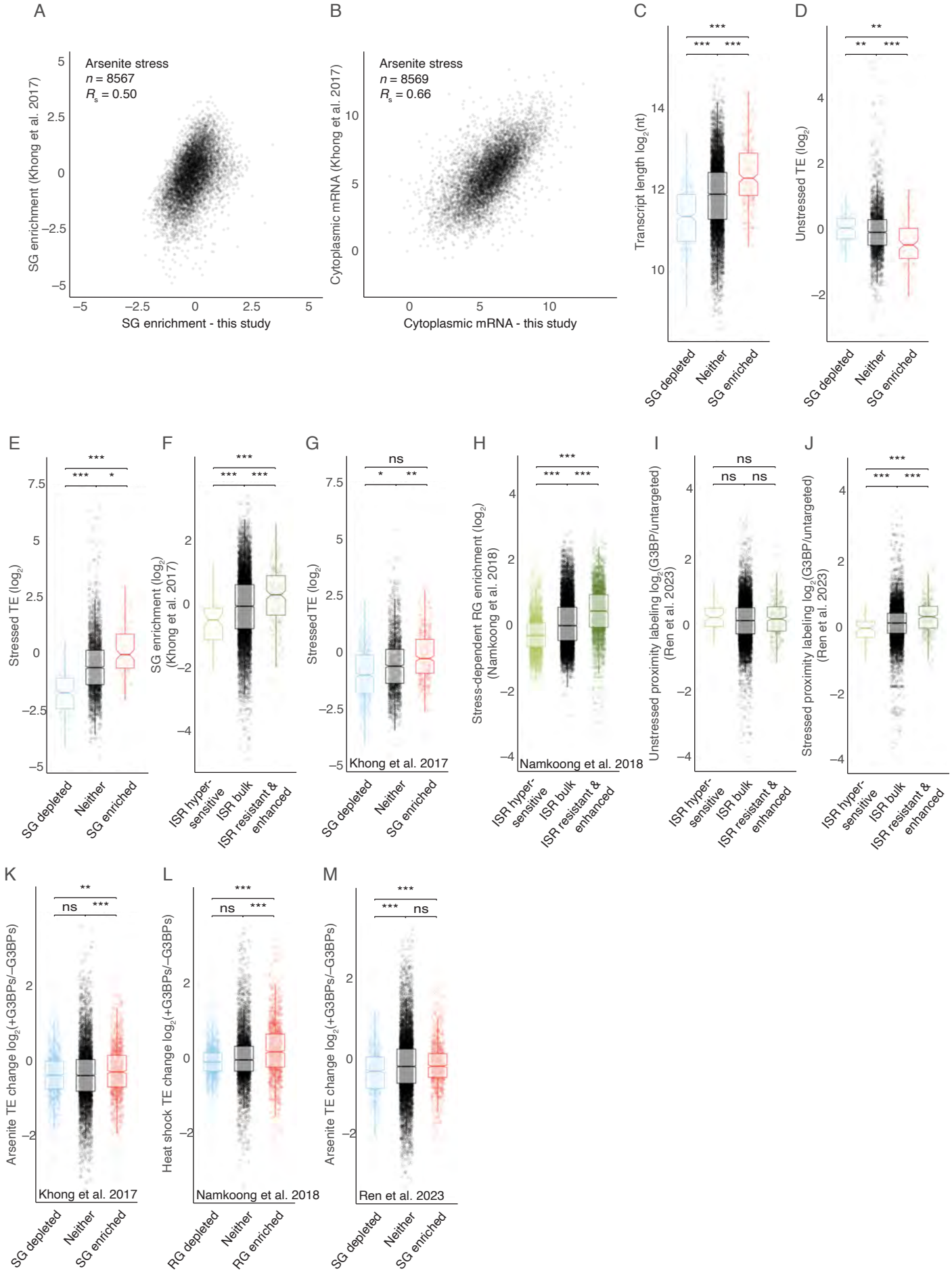
A
Arsenite stress
n = 8567
Rs = 0.50
SG enrichment (Khong et al. 2017)
SG enrichment - this study
B
Arsenite stress
n = 8569
Rs = 0.66
Cytoplasmic mRNA (Khong et al. 2017)
Cytoplasmic mRNA - this study
C
Transcript length log2(nt)
SG depleted
Neither
SG enriched
D
Unstressed TE (log2)
E
Stressed TE (log2)
F
SG enrichment (log2) (Khong et al. 2017)
ISR hyper-sensitive
ISR bulk
ISR resistant & enhanced
G
Stressed TE (log2)
Khong et al. 2017
H
Stress-dependent RG enrichment (log2) (Namkoong et al. 2018)
Namkoong et al. 2018
I
Unstressed proximity labeling log2(G3BP/untargeted) (Ren et al. 2023)
J
Stressed proximity labeling log2(G3BP/untargeted) (Ren et al. 2023)
K
Arsenite TE change log2(+G3BPs/−G3BPs)
Khong et al. 2017
L
Heat shock TE change log2(+G3BPs/−G3BPs)
Namkoong et al. 2018
RG depleted
RG enriched
M
Arsenite TE change log2(+G3BPs/−G3BPs)
Ren et al. 2023
ns

Figure S3. Conclusions regarding SG-enrichment are consistent across multiple cell types and stresses. (A) Comparison of SG enrichments. Shown are SG enrichments calculated in Khong et al. (2017)[18] plotted as a function of SG enrichments calculated in this study. *n* indicates total number of unique mRNAs. **(B)** Comparison of mRNA levels for the cells used in (A). Shown are relative mRNA abundances in U2OS cells, as measured by Khong et al. (2017)[18], plotted as a function of relative abundance in HCT116 cells, as measured in this study. Otherwise as in (A). **(C – E)** SG enrichment determinants. Shown is the relationship between either transcript length (C), unstressed TE (D), or stressed TE (E) and SG enrichment; otherwise as in Fig 3C (* $p \leq 0.05$**,** ** $p \leq 0.01$**,** *** $p \leq 0.001$). **(F)** Comparison of SG enrichment in arsenite-stressed U2OS cells as measured by Khong et al. (2017)[18] and ISR translation in arsenite stressed HCT116 cells; otherwise, as in Fig 3B. **(G)** Comparison of arsenite-stressed TE in HCT116 cells and SG enrichment in arsenite-stressed U2OS cells as measured by Khong et al. (2017)[18]; otherwise, as in (E). **(H)** Comparison of Stress-Dependent RNP Granule (RG) enrichment and ISR translation in ER-stressed NIH 3T3 cells as measured by Namkoong et al. (2018);[53] otherwise, as in (F). **(I)** Comparison of G3BP-depdenent proximity labeling in unstressed HEK293T cells as measured by Ren et al. (2023)[54] and ISR translation in arsenite stressed HCT116 cells. ns, not significant; otherwise, as in (F). **(J)** Comparison of G3BP-depdenent proximity labeling in arsenite-stressed HEK293T cells as measured by Ren et al. (2023)[54] and ISR translation in arsenite-stressed HCT116 cells; otherwise, as in (I). **(K)** Comparison of G3BP-dependent translation in HCT116 cells and SG enrichment in U2OS cells as measured by Khong et al. (2017)[18]. All stresses were 500 µM sodium arsenite for 1 h; otherwise, as in (E). **(L)** Comparison of G3BP-dependent translation in HCT116 cells and RG enrichment in NIH 3T3 cells as measured by Namkoong et al. (2018).[53] All stresses were heat shock; otherwise, as in (I). **(M)** Comparison of G3BP-dependent translation in HCT116 cells and G3BP-depdenent proximity labeling in stressed HEK293T cells as measured by Ren et al. (2023)[54]. All stresses were 500 µM sodium arsenite for 1 h; otherwise, as in (K).

Figure S4

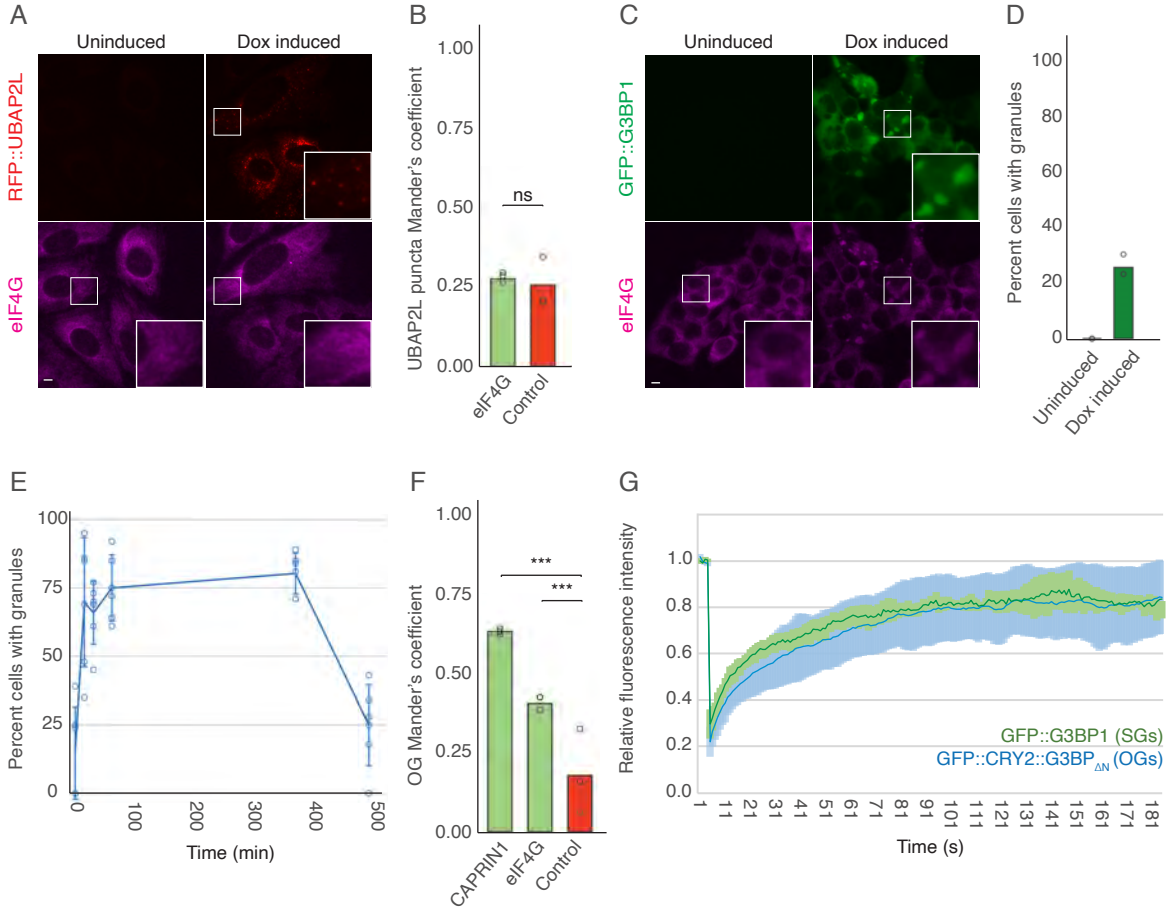
A
Uninduced
Dox induced
RFP::UBAP2L
eIF4G
B
UBAP2L puncta Mander's coefficient
1.00
0.75
0.50
0.25
0.00
ns
eIF4G
Control
C
Uninduced
Dox induced
GFP::G3BP1
eIF4G
D
Percent cells with granules
100
80
60
40
20
0
Uninduced
Dox induced
E
Percent cells with granules
100
75
50
25
0
0
100
200
300
400
500
Time (min)
F
OG Mander's coefficient
1.00
0.75
0.50
0.25
0.00
***
***
CAPRIN1
eIF4G
Control
G
Relative fluorescence intensity
1.0
0.8
0.6
0.4
0.2
0.0
GFP::G3BP1 (SGs)
GFP::CRY2::G3BP$_{\Delta N}$ (OGs)
1
11
21
31
41
51
61
71
81
91
101
111
121
131
141
151
161
171
181
Time (s)

Figure S4. OGs are SG-like condensates formed in the absence of stress. (A) No induction of ectopic SGs caused by UBAP2L overexpression. Unstressed U2OS cells were either treated with 1 µM doxycycline (right) or not treated (left) to induce overexpression of UBAP2L. Images show either UBAP2L in red or SG marker protein eIF4G in magenta (scale bars, 10 µm). White boxes highlight insets that are expanded on the right. **(B)** Colocalization of UBAP2L puncta with SG marker. Quantification of colocalization was performed using Mander's coefficient between UBAP2L and eIF4G as an SG marker, comparing to a control image from an irrelevant field of cells (***, $p \leq 0.001$; Welch's two-sample t-test)**. (C)** Induction of ectopic SGs caused by G3BP overexpression. Unstressed HCT116 cells were either treated with 1 µM doxycycline (right) or not treated (left) to induce overexpression of G3BP1. Images show either G3BP1 in green or SG marker protein eIF4G in magenta; otherwise, as in (A). **(D)** Quantification of ectopic granule formation in (C). Points indicate values for three biological replicates. **(E)** Kinetics of OG formation and dissolution. Plotted over time is the percent of cells with visible OGs. Cells were exposed to blue light starting at 0 min and removed from blue light at 360 min. Error bars report standard deviation for six biological replicates shown as points. **(F)** Colocalization of SG markers in OGs. Quantification of colocalization was performed using Mander's coefficient between GFP::CRY2::G3BP$_{\Delta N}$ and indicated SG marker, comparing to a control image from an irrelevant field of cells (***, $p \leq 0.001$; Welch's two-sample t-test)**. (G)** FRAP of OGs. Plotted over time is the fluorescence intensity of GFP-labeled granules after photobleaching. SG (green) and OG (blue) recoveries are shown over a 180 s time course. Photobleaching occurred at 3 s. Error bars report standard deviation for at least six granules from at least three cells.

Figure S5

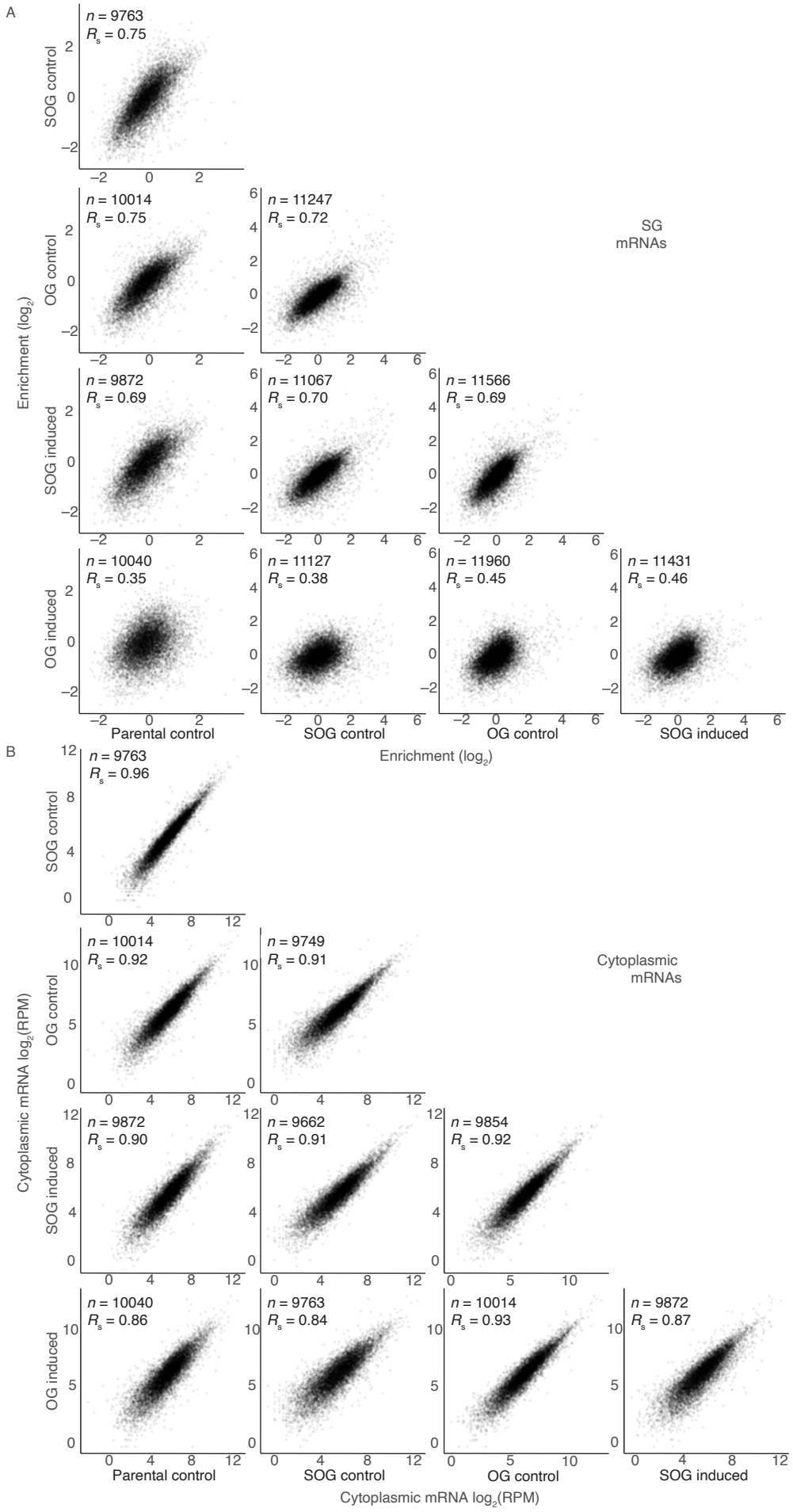
A
n = 9763
Rs = 0.75
n = 10014
Rs = 0.75
n = 11247
Rs = 0.72
SG
mRNAs
n = 9872
Rs = 0.69
n = 11067
Rs = 0.70
n = 11566
Rs = 0.69
n = 10040
Rs = 0.35
n = 11127
Rs = 0.38
n = 11960
Rs = 0.45
n = 11431
Rs = 0.46
Enrichment (log2)
SOG control
OG control
SOG induced
OG induced
Parental control
SOG control
OG control
SOG induced
Enrichment (log2)
B
n = 9763
Rs = 0.96
n = 10014
Rs = 0.92
n = 9749
Rs = 0.91
Cytoplasmic
mRNAs
n = 9872
Rs = 0.90
n = 9662
Rs = 0.91
n = 9854
Rs = 0.92
n = 10040
Rs = 0.86
n = 9763
Rs = 0.84
n = 10014
Rs = 0.93
n = 9872
Rs = 0.87
Cytoplasmic mRNA log2(RPM)
SOG control
OG control
SOG induced
OG induced
Parental control
SOG control
OG control
SOG induced
Cytoplasmic mRNA log2(RPM)

Figure S5. OGs require stress to recruit the SG transcriptome. (A) Expanded comparisons of granule enrichment, showing the distributions used to calculate the R_S values of Fig 5E. *n* indicates total number of unique mRNAs. **(B)** Expanded comparisons of cell line transcriptomes, showing the distributions used to calculate the R_S values of Fig 5F.

Figure S6

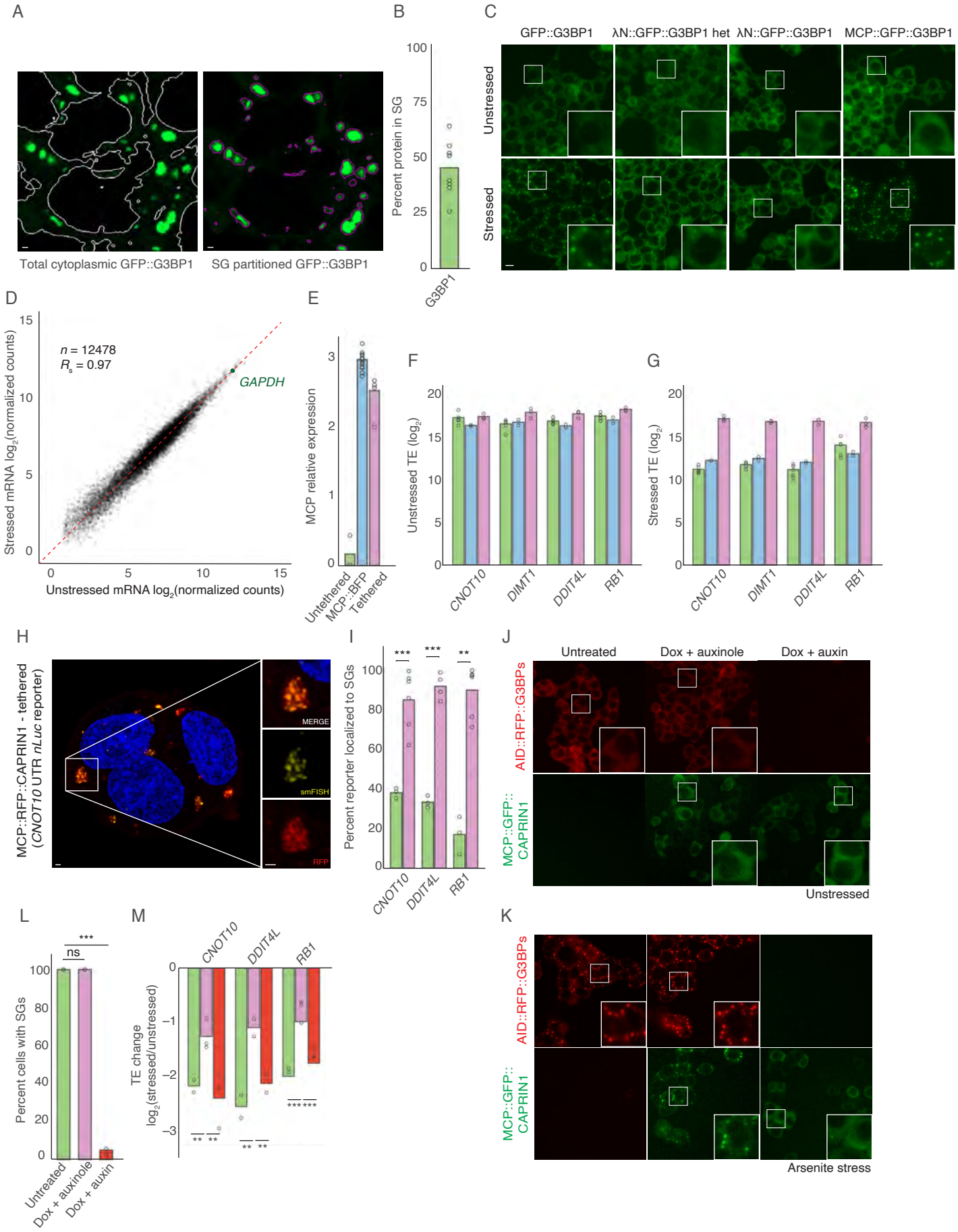
A
Total cytoplasmic GFP::G3BP1
SG partitioned GFP::G3BP1
B
Percent protein in SG
G3BP1
C
GFP::G3BP1
λN::GFP::G3BP1 het
λN::GFP::G3BP1
MCP::GFP::G3BP1
Unstressed
Stressed
D
n = 12478
Rs = 0.97
GAPDH
Stressed mRNA log2(normalized counts)
Unstressed mRNA log2(normalized counts)
E
MCP relative expression
Untethered
MCP::BFP
Tethered
F
Unstressed TE (log2)
CNOT10
DIMT1
DDIT4L
RB1
G
Stressed TE (log2)
CNOT10
DIMT1
DDIT4L
RB1
H
MCP::RFP::CAPRIN1 - tethered
(CNOT10 UTR nLuc reporter)
MERGE
smFISH
RFP
I
Percent reporter localized to SGs
CNOT10
DDIT4L
RB1
J
Untreated
Dox + auxinole
Dox + auxin
AID::RFP::G3BPs
MCP::GFP::
CAPRIN1
Unstressed
K
AID::RFP::G3BPs
MCP::GFP::
CAPRIN1
Arsenite stress
L
Percent cells with SGs
ns
Untreated
Dox + auxinole
Dox + auxin
M
CNOT10
DDIT4L
RB1
TE change
log2(stressed/unstressed)

Figure S6. Tethering to SGs via CAPRIN1 imparts G3BP-dependent resistance to ISR translation shutdown. (A) G3BP1 partitioning to SGs. HCT116 cells expressing G3BP1 endogenously tagged with GFP were stressed with 500 µM sodium arsenite for 90 min. Images show localization of G3BP in green. White outlines show cell boundaries as determined by Imaris software based on cytosolic fluorescence. Purple outlines show SG boundaries as determined by Imaris software (scale bars, 1 µm). **(B)** Quantification of G3BP1 partitioning to SGs. Points show the amount of fluorescence from SGs as a percent of total fluorescence, for eight independent replicates each containing at least three cells. **(C)** Effects of tagging G3BP with λN and MCP. HCT116 cells expressing endogenous G3BP tagged with the indicated GFP fusion protein were either unstressed (top) or treated with 500 µM sodium arsenite for 1 h (bottom) to assess SG formation (scale bar, 10 µm). White boxes highlight insets that are expanded on the right. **(D)** mRNA changes during stress. Plotted for each mRNA is its abundance in arsenite-stressed HCT116 cells (500 µM sodium arsenite for 1 h) as a function of its abundance in unstressed HCT116 cells. The *GAPDH* mRNA, which was used as a control for RT-qPCR, is highlighted in green. The red dashed line indicates unchanged abundance. *n* indicates total number of unique mRNAs. **(E)** Quantification of MCP expression. Plot indicates relative MCP expression as determined by RT-qPCR in HCT116 cell lines expressing either endogenously tagged GFP::G3BP (untethered), GFP::G3BP and MCP::BFP (MCP::BFP), or MCP::GFP::G3BP (tethered). The points show values of at least three biological replicates. **(F)** Unstressed SG-tethered translation response. Plotted for each reporter is the unstressed $\log_2$ TE in either untethered cells (green), untethered cells expressing MCP::BFP (blue), or tethered cells (pink). **(G)** Stressed SG-tethered translation response. Plotted for each reporter is the stressed $\log_2$ TE; otherwise, as in (F). **(H)** Tethering a luciferase reporter to SGs via CAPRIN1. HCT116 cells expressing a NanoLuc reporter bearing 5' and 3' UTRs from *CNOT10* and MCP::RFP::CAPRIN1 were stressed with 500 µM sodium arsenite for 90 min. Images show localization of CAPRIN1 in red and smFISH of NanoLuc reporter molecules in yellow (scale bars, 1 µm). White boxes highlight insets that are expanded on the right. **(I)** SG tethering efficiency. Percent of cytoplasmic reporter molecules localized to SGs in untethered cells (replotted from Figure 6C in green) and to SGs in CAPRIN1-tethered cells (pink) are shown for reporters with 5' and 3' UTRs of the indicated genes. Points show values for at least three biological replicates (** $p \leq 0.01$, *** $p \leq 0.001$, Welch's two-sample t-test). The average SG tethering efficiency for the four different reporters was 30% for untethered cells and 89% for tethered cells, with standard deviations of 11% and 4%, respectively. **(J)** Cells expressing CAPRIN1 tether while depleted of G3BPs. HCT116 cells expressing endogenously tagged AID::RFP::G3BPs were either untreated (left), treated with 1 µM doxycycline and 200 µM auxinole for 10 h, leading to retention of G3BPs and expression of MCP::GFP::CAPRIN1 (middle), or treated with 1 µM doxycycline and 500 µM IAA for 10 h, leading to turnover of endogenous G3BPs and expression of MCP::GFP::CAPRIN1 (right). Otherwise as in (C). **(K)** Assessment of SG formation in cells expressing CAPRIN1 tether while depleted of G3BPs. Cells were treated as in (J) and then subsequently stressed with 500 µM sodium arsenite for 90 min; otherwise, as in (J). **(L)** Quantification of granule formation in (K). Error bars report standard deviation for three biological replicates (*** $p \leq 0.001$, ns, not significant, Welch's two-sample t-test). **(M)** CAPRIN1-tethered ISR translation response. Plotted for each reporter is the change in TE caused by arsenite stress (500 µM sodium arsenite for 90 min) in untethered cells (green), tethered cells expressing G3BPs (pink), or tethered cells depleted of G3BPs (red) (*** $p \leq 0.001$, ** $p \leq$

0.01, ns, not significant, Welch's two-sample t-test). The average $\log_2$ FC in TE for the ISR translation response was –2.24 for untethered cells, –1.12 for CAPRIN1-tethered cells expressing G3BPs, and –2.09 for CAPRIN1-tethered cells depleted of G3BPs.

Table S1

RNA	Endogenous TE change $\log_2$(stressed/unstressed)	Reporter TE change $\log_2$(stressed/unstressed)
CNOT10	–4.44	–5.49
DIMT1	–1.82	–4.42
DDIT4L	4.18	–5.362
RB1	–2.24	–3.24

1206 **Table S1. Luciferase reporters do not recapitulate endogenous TE behavior.** Listed for each
1207 mRNA are endogenous changes in TE due to presence of arsenite stress (500 µM sodium
1208 arsenite for 1 h), and reporter changes in TE due to presence of arsenite stress (500 µM sodium
1209 arsenite for 1.5 h).
1210
1211
1212
1213
1214
1215
1216
1217
1218
1219
1220
1221
1222
1223
1224
1225
1226
1227
1228
1229

1230 1 Kedersha, N. *et al.* G3BP-Caprin1-USP10 complexes mediate stress granule condensation
1231 and associate with 40S subunits. *J Cell Biol* **212**, 845-860, doi:10.1083/jcb.201508028
1232 (2016).
1233 2 Yang, P. *et al.* G3BP1 Is a Tunable Switch that Triggers Phase Separation to Assemble
1234 Stress Granules. *Cell* **181**, 325-345 e328, doi:10.1016/j.cell.2020.03.046 (2020).
1235 3 Sanders, D. W. *et al.* Competing Protein-RNA Interaction Networks Control Multiphase
1236 Intracellular Organization. *Cell* **181**, 306-324 e328, doi:10.1016/j.cell.2020.03.050 (2020).
1237 4 Guillen-Boixet, J. *et al.* RNA-Induced Conformational Switching and Clustering of G3BP
1238 Drive Stress Granule Assembly by Condensation. *Cell* **181**, 346-361 e317,
1239 doi:10.1016/j.cell.2020.03.049 (2020).
1240 5 Buchan, J. R. & Parker, R. Eukaryotic stress granules: the ins and outs of translation. *Mol*
1241 *Cell* **36**, 932-941, doi:10.1016/j.molcel.2009.11.020 (2009).
1242 6 Advani, V. M. & Ivanov, P. Translational Control under Stress: Reshaping the Translatome.
1243 *Bioessays* **41**, e1900009, doi:10.1002/bies.201900009 (2019).
1244 7 Pakos-Zebrucka, K. *et al.* The integrated stress response. *EMBO Rep* **17**, 1374-1395,
1245 doi:10.15252/embr.201642195 (2016).
1246 8 Harding, H. P. *et al.* Regulated translation initiation controls stress-induced gene
1247 expression in mammalian cells. *Mol Cell* **6**, 1099-1108, doi:10.1016/s1097-
1248 2765(00)00108-8 (2000).
1249 9 Harding, H. P., Zhang, Y. & Ron, D. Protein translation and folding are coupled by an
1250 endoplasmic-reticulum-resident kinase. *Nature* **397**, 271-274, doi:10.1038/16729
1251 (1999).
1252 10 Yamasaki, S. & Anderson, P. Reprogramming mRNA translation during stress. *Curr Opin*
1253 *Cell Biol* **20**, 222-226, doi:10.1016/j.ceb.2008.01.013 (2008).
1254 11 Starck, S. R. *et al.* Translation from the 5' untranslated region shapes the integrated
1255 stress response. *Science* **351**, aad3867, doi:10.1126/science.aad3867 (2016).
1256 12 Sidrauski, C., McGeachy, A. M., Ingolia, N. T. & Walter, P. The small molecule ISRIB
1257 reverses the effects of eIF2alpha phosphorylation on translation and stress granule
1258 assembly. *Elife* **4**, doi:10.7554/eLife.05033 (2015).
1259 13 Vattem, K. M. & Wek, R. C. Reinitiation involving upstream ORFs regulates ATF4 mRNA
1260 translation in mammalian cells. *Proc Natl Acad Sci U S A* **101**, 11269-11274,
1261 doi:10.1073/pnas.0400541101 (2004).
1262 14 Protter, D. S. W. & Parker, R. Principles and Properties of Stress Granules. *Trends Cell Biol*
1263 **26**, 668-679, doi:10.1016/j.tcb.2016.05.004 (2016).
1264 15 Kedersha, N. L., Gupta, M., Li, W., Miller, I. & Anderson, P. RNA-binding Proteins TIA-1
1265 and TIAR Link the Phosphorylation of eIF-2 to the Assembly of Mammalian Stress
1266 Granules. *The Journal of Cell Biology* **147**, 1431-1441 (1999).
1267 16 Molliex, A. *et al.* Phase separation by low complexity domains promotes stress granule
1268 assembly and drives pathological fibrillization. *Cell* **163**, 123-133,
1269 doi:10.1016/j.cell.2015.09.015 (2015).
1270 17 Jain, S. *et al.* ATPase-Modulated Stress Granules Contain a Diverse Proteome and
1271 Substructure. *Cell* **164**, 487-498, doi:10.1016/j.cell.2015.12.038 (2016).

18 Khong, A. *et al.* The Stress Granule Transcriptome Reveals Principles of mRNA Accumulation in Stress Granules. *Mol Cell* **68**, 808-820 e805, doi:10.1016/j.molcel.2017.10.015 (2017).

19 Markmiller, S. *et al.* Context-Dependent and Disease-Specific Diversity in Protein Interactions within Stress Granules. *Cell* **172**, 590-604 e513, doi:10.1016/j.cell.2017.12.032 (2018).

20 Kedersha, N. *et al.* Evidence That Ternary Complex (eIF2-GTP-tRNAiMet)-Deficient Preinitiation Complexes Are Core Constituents of Mammalian Stress Granules. *Molecular Biology of the Cell* **13**, 195-210, doi:10.1091/mbc.01-05-0221 (2002).

21 Laver, J. D. *et al.* The RNA-Binding Protein Rasputin/G3BP Enhances the Stability and Translation of Its Target mRNAs. *Cell Rep* **30**, 3353-3367 e3357, doi:10.1016/j.celrep.2020.02.066 (2020).

22 Alam, U. & Kennedy, D. Rasputin a decade on and more promiscuous than ever? A review of G3BPs. *Biochim Biophys Acta Mol Cell Res* **1866**, 360-370, doi:10.1016/j.bbamcr.2018.09.001 (2019).

23 Meyer, C., Garzia, A., Morozov, P., Molina, H. & Tuschl, T. The G3BP1-Family-USP10 Deubiquitinase Complex Rescues Ubiquitinated 40S Subunits of Ribosomes Stalled in Translation from Lysosomal Degradation. *Mol Cell* **77**, 1193-1205 e1195, doi:10.1016/j.molcel.2019.12.024 (2020).

24 Anderson, P. & Kedersha, N. RNA granules: post-transcriptional and epigenetic modulators of gene expression. *Nat Rev Mol Cell Biol* **10**, 430-436, doi:10.1038/nrm2694 (2009).

25 Kedersha, N. *et al.* Dynamic shuttling of TIA-1 accompanies the recruitment of mRNA to mammalian stress granules. *J Cell Biol* **151**, 1257-1268, doi:10.1083/jcb.151.6.1257 (2000).

26 Kwon, S., Zhang, Y. & Matthias, P. The deacetylase HDAC6 is a novel critical component of stress granules involved in the stress response. *Genes Dev* **21**, 3381-3394, doi:10.1101/gad.461107 (2007).

27 Youn, J. Y. *et al.* Properties of Stress Granule and P-Body Proteomes. *Mol Cell* **76**, 286-294, doi:10.1016/j.molcel.2019.09.014 (2019).

28 Kimball, S. R., Horetsky, R. L., Ron, D., Jefferson, L. S. & Harding, H. P. Mammalian stress granules represent sites of accumulation of stalled translation initiation complexes. *Am J Physiol Cell Physiol* **284**, C273-284, doi:10.1152/ajpcell.00314.2002 (2003).

29 Moon, S. L. *et al.* Multicolour single-molecule tracking of mRNA interactions with RNP granules. *Nat Cell Biol* **21**, 162-168, doi:10.1038/s41556-018-0263-4 (2019).

30 Mateju, D. *et al.* Single-Molecule Imaging Reveals Translation of mRNAs Localized to Stress Granules. *Cell* **183**, 1801-1812 e1813, doi:10.1016/j.cell.2020.11.010 (2020).

31 Tourriere, H. *et al.* The RasGAP-associated endoribonuclease G3BP assembles stress granules. *J Cell Biol* **160**, 823-831, doi:10.1083/jcb.200212128 (2003).

32 Zhang, P. *et al.* Chronic optogenetic induction of stress granules is cytotoxic and reveals the evolution of ALS-FTD pathology. *Elife* **8**, doi:10.7554/eLife.39578 (2019).

33 Baymiller, M. & Moon, S. L. Stress Granules as Causes and Consequences of Translation Suppression. *Antioxid Redox Signal* **39**, 390-409, doi:10.1089/ars.2022.0164 (2023).

34 Putnam, A., Thomas, L. & Seydoux, G. RNA granules: functional compartments or incidental condensates? *Genes Dev* **37**, 354-376, doi:10.1101/gad.350518.123 (2023).

35 Mateju, D. & Chao, J. A. Stress granules: regulators or by-products? *FEBS J* **289**, 363-373, doi:10.1111/febs.15821 (2022).

36 Ingolia, N. T. Ribosome Footprint Profiling of Translation throughout the Genome. *Cell* **165**, 22-33, doi:10.1016/j.cell.2016.02.066 (2016).

37 Iwasaki, S., Floor, S. N. & Ingolia, N. T. Rocaglates convert DEAD-box protein eIF4A into a sequence-selective translational repressor. *Nature* **534**, 558-561, doi:10.1038/nature17978 (2016).

38 Wilbertz, J. H. *et al.* Single-Molecule Imaging of mRNA Localization and Regulation during the Integrated Stress Response. *Mol Cell* **73**, 946-958 e947, doi:10.1016/j.molcel.2018.12.006 (2019).

39 Aulas, A. *et al.* Stress-specific differences in assembly and composition of stress granules and related foci. *J Cell Sci* **130**, 927-937, doi:10.1242/jcs.199240 (2017).

40 Sonenberg, N. & Hinnebusch, A. G. Regulation of translation initiation in eukaryotes: mechanisms and biological targets. *Cell* **136**, 731-745, doi:10.1016/j.cell.2009.01.042 (2009).

41 Holcik, M. & Sonenberg, N. Translational control in stress and apoptosis. *Nat Rev Mol Cell Biol* **6**, 318-327, doi:10.1038/nrm1618 (2005).

42 Andreev, D. E. *et al.* Translation of 5' leaders is pervasive in genes resistant to eIF2 repression. *Elife* **4**, e03971, doi:10.7554/eLife.03971 (2015).

43 Chen, J., Brunner, A.-D., Nunez, J. K. & Weissman, J. Pervasive functional translation of noncanonical human open reading frames. *Science* **367**, 1135-1140, doi:10.1126/science.aay0262 (2020).

44 Glauninger, H. *et al.* Transcriptome-wide mRNA condensation precedes stress granule formation and excludes stress-induced transcripts. *bioRxiv*, doi:10.1101/2024.04.15.589678 (2024).

45 Mostafa Zedan, A. P. S., Stephanie Heinrich, Pablo Aurelio Gómez García, Sarah Khawaja, Karsten Weis. Newly synthesized mRNA selectively escapes translational repression following acute stress. *bioRxiv*, doi:https://doi.org/10.1101/2024.04.14.589419 (2024).

46 Agarwal, V. & Kelley, D. R. The genetic and biochemical determinants of mRNA degradation rates in mammals. *Genome Biology* **23**, 245, doi:10.1186/s13059-022-02811-x (2022).

47 Pizzinga, M. *et al.* The cell stress response: extreme times call for post-transcriptional measures. *Wiley Interdiscip Rev RNA* **11**, e1578, doi:10.1002/wrna.1578 (2020).

48 Natsume, T., Kiyomitsu, T., Saga, Y. & Kanemaki, M. T. Rapid Protein Depletion in Human Cells by Auxin-Inducible Degron Tagging with Short Homology Donors. *Cell Rep* **15**, 210-218, doi:10.1016/j.celrep.2016.03.001 (2016).

49 Nishimura, K., Fukagawa, T., Takisawa, H., Kakimoto, T. & Kanemaki, M. An auxin-based degron system for the rapid depletion of proteins in nonplant cells. *Nat Methods* **6**, 917-922, doi:10.1038/nmeth.1401 (2009).

50 Cirillo, L. *et al.* UBAP2L Forms Distinct Cores that Act in Nucleating Stress Granules Upstream of G3BP1. *Curr Biol* **30**, 698-707 e696, doi:10.1016/j.cub.2019.12.020 (2020).

1358 51 Paget, M. *et al.* Stress granules are shock absorbers that prevent excessive innate
1359 immune responses to dsRNA. *Mol Cell* **83**, 1180-1196 e1188,
1360 doi:10.1016/j.molcel.2023.03.010 (2023).
1361 52 Khong, A., Jain, S., Matheny, T., Wheeler, J. R. & Parker, R. Isolation of mammalian stress
1362 granule cores for RNA-Seq analysis. *Methods* **137**, 49-54,
1363 doi:10.1016/j.ymeth.2017.11.012 (2018).
1364 53 Namkoong, S., Ho, A., Woo, Y. M., Kwak, H. & Lee, J. H. Systematic Characterization of
1365 Stress-Induced RNA Granulation. *Mol Cell* **70**, 175-187 e178,
1366 doi:10.1016/j.molcel.2018.02.025 (2018).
1367 54 Ren, Z., Tang, W., Peng, L. & Zou, P. Profiling stress-triggered RNA condensation with
1368 photocatalytic proximity labeling. *Nat Commun* **14**, 7390, doi:10.1038/s41467-023-
1369 43194-2 (2023).
1370 55 Huang, C. *et al.* UBAP2L arginine methylation by PRMT1 modulates stress granule
1371 assembly. *Cell Death Differ* **27**, 227-241, doi:10.1038/s41418-019-0350-5 (2020).
1372 56 Panas, M. D., Ivanov, P. & Anderson, P. Mechanistic insights into mammalian stress
1373 granule dynamics. *J Cell Biol* **215**, 313-323, doi:10.1083/jcb.201609081 (2016).
1374 57 Ivanov, P., Kedersha, N. & Anderson, P. Stress Granules and Processing Bodies in
1375 Translational Control. *Cold Spring Harb Perspect Biol* **11**,
1376 doi:10.1101/cshperspect.a032813 (2019).
1377 58 Matheny, T., Rao, B. S. & Parker, R. Transcriptome-Wide Comparison of Stress Granules
1378 and P-Bodies Reveals that Translation Plays a Major Role in RNA Partitioning. *Mol Cell*
1379 *Biol* **39**, doi:10.1128/MCB.00313-19 (2019).
1380 59 Lee, C. S. *et al.* Recruitment of mRNAs to P granules by condensation with intrinsically-
1381 disordered proteins. *Elife* **9**, doi:10.7554/eLife.52896 (2020).
1382 60 Ramadurgum, P. & Hulleman, J. D. Protocol for Designing Small-Molecule-Regulated
1383 Destabilizing Domains for In Vitro Use. *STAR Protoc* **1**, doi:10.1016/j.xpro.2020.100069
1384 (2020).
1385 61 Bertrand, E. *et al.* Localization of ASH1 mRNA particles in living yeast. *Mol Cell* **2**, 437-
1386 445, doi:10.1016/s1097-2765(00)80143-4 (1998).
1387 62 Wheeler, J. R., Jain, S., Khong, A. & Parker, R. Isolation of yeast and mammalian stress
1388 granule cores. *Methods* **126**, 12-17, doi:10.1016/j.ymeth.2017.04.020 (2017).
1389 63 Matheny, T., Van Treeck, B., Huynh, T. N. & Parker, R. RNA partitioning into stress
1390 granules is based on the summation of multiple interactions. *RNA* **27**, 174-189,
1391 doi:10.1261/rna.078204.120 (2021).
1392 64 Khong, A., Matheny, T., Huynh, T. N., Babl, V. & Parker, R. Limited effects of m(6)A
1393 modification on mRNA partitioning into stress granules. *Nat Commun* **13**, 3735,
1394 doi:10.1038/s41467-022-31358-5 (2022).
1395 65 Burke, J. M., Moon, S. L., Matheny, T. & Parker, R. RNase L Reprograms Translation by
1396 Widespread mRNA Turnover Escaped by Antiviral mRNAs. *Mol Cell* **75**, 1203-1217 e1205,
1397 doi:10.1016/j.molcel.2019.07.029 (2019).
1398 66 Burke, J. M., Ratnayake, O. C., Watkins, J. M., Perera, R. & Parker, R. G3BP1-dependent
1399 condensation of translationally inactive viral RNAs antagonizes infection. *Sci Adv* **10**,
1400 eadk8152, doi:10.1126/sciadv.adk8152 (2024).

1401 67 Burke, J. M., Lester, E. T., Tauber, D. & Parker, R. RNase L promotes the formation of
1402 unique ribonucleoprotein granules distinct from stress granules. *J Biol Chem* **295**, 1426-
1403 1438, doi:10.1074/jbc.RA119.011638 (2020).
1404 68 Buchan, J. R., Muhlrad, D. & Parker, R. P bodies promote stress granule assembly in
1405 Saccharomyces cerevisiae. *J Cell Biol* **183**, 441-455, doi:10.1083/jcb.200807043 (2008).
1406 69 Fedorovskiy, A. G. *et al.* A Solitary Stalled 80S Ribosome Prevents mRNA Recruitment to
1407 Stress Granules. *Biochemistry (Mosc)* **88**, 1786-1799, doi:10.1134/S000629792311010X
1408 (2023).
1409 70 Luo, E. C. *et al.* Large-scale tethered function assays identify factors that regulate mRNA
1410 stability and translation. *Nat Struct Mol Biol* **27**, 989-1000, doi:10.1038/s41594-020-
1411 0477-6 (2020).
1412 71 Bidet, K., Dadlani, D. & Garcia-Blanco, M. A. G3BP1, G3BP2 and CAPRIN1 are required for
1413 translation of interferon stimulated mRNAs and are targeted by a dengue virus non-
1414 coding RNA. *PLoS Pathog* **10**, e1004242, doi:10.1371/journal.ppat.1004242 (2014).
1415 72 Ortega, A. D., Willers, I. M., Sala, S. & Cuezva, J. M. Human G3BP1 interacts with beta-F1-
1416 ATPase mRNA and inhibits its translation. *J Cell Sci* **123**, 2685-2696,
1417 doi:10.1242/jcs.065920 (2010).
1418 73 Wheeler, J. R., Matheny, T., Jain, S., Abrisch, R. & Parker, R. Distinct stages in stress
1419 granule assembly and disassembly. *Elife* **5**, doi:10.7554/eLife.18413 (2016).
1420 74 Downey, N. Extraction of DNA from agarose gels. *Methods Mol Biol* **235**, 137-139,
1421 doi:10.1385/1-59259-409-3:137 (2003).
1422 75 Yesbolatova, A., Natsume, T., Hayashi, K. I. & Kanemaki, M. T. Generation of conditional
1423 auxin-inducible degron (AID) cells and tight control of degron-fused proteins using the
1424 degradation inhibitor auxinole. *Methods* **164-165**, 73-80,
1425 doi:10.1016/j.ymeth.2019.04.010 (2019).
1426 76 Xiang, K. & Bartel, D. P. The molecular basis of coupling between poly(A)-tail length and
1427 translational efficiency. *Elife* **10**, doi:10.7554/eLife.66493 (2021).
1428 77 Subtelny, A. O., Eichhorn, S. W., Chen, G. R., Sive, H. & Bartel, D. P. Poly(A)-tail profiling
1429 reveals an embryonic switch in translational control. *Nature* **508**, 66-71,
1430 doi:10.1038/nature13007 (2014).
1431 78 Love, M. I., Huber, W. & Anders, S. Moderated estimation of fold change and dispersion
1432 for RNA-seq data with DESeq2. *Genome Biol* **15**, 550, doi:10.1186/s13059-014-0550-8
1433 (2014).
1434